Dry Metal Forming Open Access Journal

Final Project Report

Edited by Frank Vollertsen
Available online at https://elib.suub.uni-bremen.de

www.drymetalforming.de

Dry Met. Forming OAJ FPR 6 (2020) 030–068
Date of Report 31 May 2020; published 12 June 2020

Macro- and microstructuring of deep drawing tools for dry forming processes

(DFG Grant No. LA 2513/5; BE 1875/31; BR 3500/12, Funding Period 01.01.2014 – 31.05.2020)

Theresa Jähnig[1,3], Ali Mousavi[1,2], Teja Roch[5], Eckhart Beyer[1,5], Andrés F. Lasagni[1,5], Alexander Brosius*[1,2]

[1] Institut für Fertigungstechnik, TU Dresden, 01062 Dresden, Germany
[2] Lehrstuhl für Formgebende Fertigungsverfahren, TU Dresden, 01062 Dresden, Germany
[3] Lehrstuhl für Laserbasierte Methoden der großflächigen Oberflächenstrukturierung, TU Dresden, 01062 Dresden, Germany
[4] Lehrstuhl für Laser- und Oberflächentechnik, TU Dresden, 01062 Dresden, Germany
[5] Fraunhofer Institut für Werkstoff- und Strahltechnik IWS, Winterbergstraße 28, 01277 Dresden, Germany

Summary

In forming processes, lubrication is needed to reduce friction and wear occurring at the contact areas between the work-piece and the tool. This is provided by separating these surfaces as well as transporting abrasive wear out of the sliding interface. With high interest in waste avoidance and efficient use of resources, today's industry aims for substituting these lubricants. Thereby, deposition of coatings or local surface structuring offer a different way to reduce friction in forming processes. For instance, this can be reached by using different hard coatings as well as by utilizing manufacturing methods capable to control and reduce the contact area in the tribological system.

In this project, the flange area of a deep drawing tool was macro-structured by turning-process (rotational symmetric geometry) and by milling-process (non rotational-symmetric part) to decrease the contact area of the work-piece up to 94% during the forming process. Also, the drawing edge radius of the tools was coated with different types of hydrogen-free tetrahedral amorphous carbon layers, e.g. with a sp^3-ratios between 60% and 70%. Together with the subsequently introduced micro-features on the ta-C layer, employing the innovative method of Direct Laser Interference Patterning (DLIP), a further reduction of the contact areas was possible as well as to produce local rehybridization of the ta-C material. Also, high-throughput surface texturing of semi-finished sheet metals by DLIP process was performed, for reducing friction by minimizing also the contact area with the deep drawing tool.

Forming of test strips showed the influence of the macro-structured flange area by reducing the friction force down to 75%. In addition, different modelling tools were developed for calculating both the process window and to determine the generation of wrinkles during deep drawing with macro-structured tools. The macro-structured deep drawing tools could also enlarge the process limits by increasing the stability against wrinkling of the sheet metal during the drawing process. The ta-C coating on the die radius without application of lubrication was capable to reduce the friction coefficient up to 20% compared to uncoated lubricated conditions. Performed tensile-bend tests on micro-structured ta-C coated cylinders also demonstrated the potential to reduce friction, as well as an excellent capability to reduce wear compared to the standard conditions.

Keywords: deep drawing, dry forming, friction reduction, micro structuring, macro structuring, diamond lioke coatings, ta-C, direct laser interference patterning, surface functionalization

*E-mail address of corresponding author: alexander.brosius@tu-dresden.de

1 Aim of the project

In metal forming and especially for deep drawing processes, lubricants are used to considerably reduce the friction between tool and workpiece. Effective lubrication is needed, as large contact areas and high normal surface pressures lead to high friction forces during the forming process. However, lubricants are often hazardous to the health and environment. Therefore, new more restrictive laws have been issued in Europe and Japan since 2000, concerning the use of harmful lubricants in industrial application to establish safe and healthy working conditions [1].

Furthermore, the application of lubricants in metal forming require subsequent cleaning of the forming parts and adequate waste disposal, which increases the production costs further [2]. A lack of lubrication leads to higher friction forces and accordingly higher punch forces in deep drawing processes. As a result, the process limiting occurrence of wrinkles and bottom cracks is more likely. Hence, the negative impact of missing lubrication has to be compensated by an adapted tool concept.

Within the scope of this project, a new lubricant-free deep drawing process was developed, which is described in Figure 1. The frictional forces and the tool wear are reduced at the critical tool areas. This is done by utilizing several strategies, including macro structuring the tool in the flange area, coating of the die edge radius with a protective layer of tetrahedral amorphous carbon (ta-C) and a subsequent micro structuring with Direct Laser Interference Patterning (DLIP) of the ta-C surface. This concept includes also the micro-structuring of the semi-finished products with a high-througput concept of DLIP, to further reduce the contact area between deep forming tool and blank.

Each of these strategies is summarized in this report, describing the most relevant results obtained along the funding period.

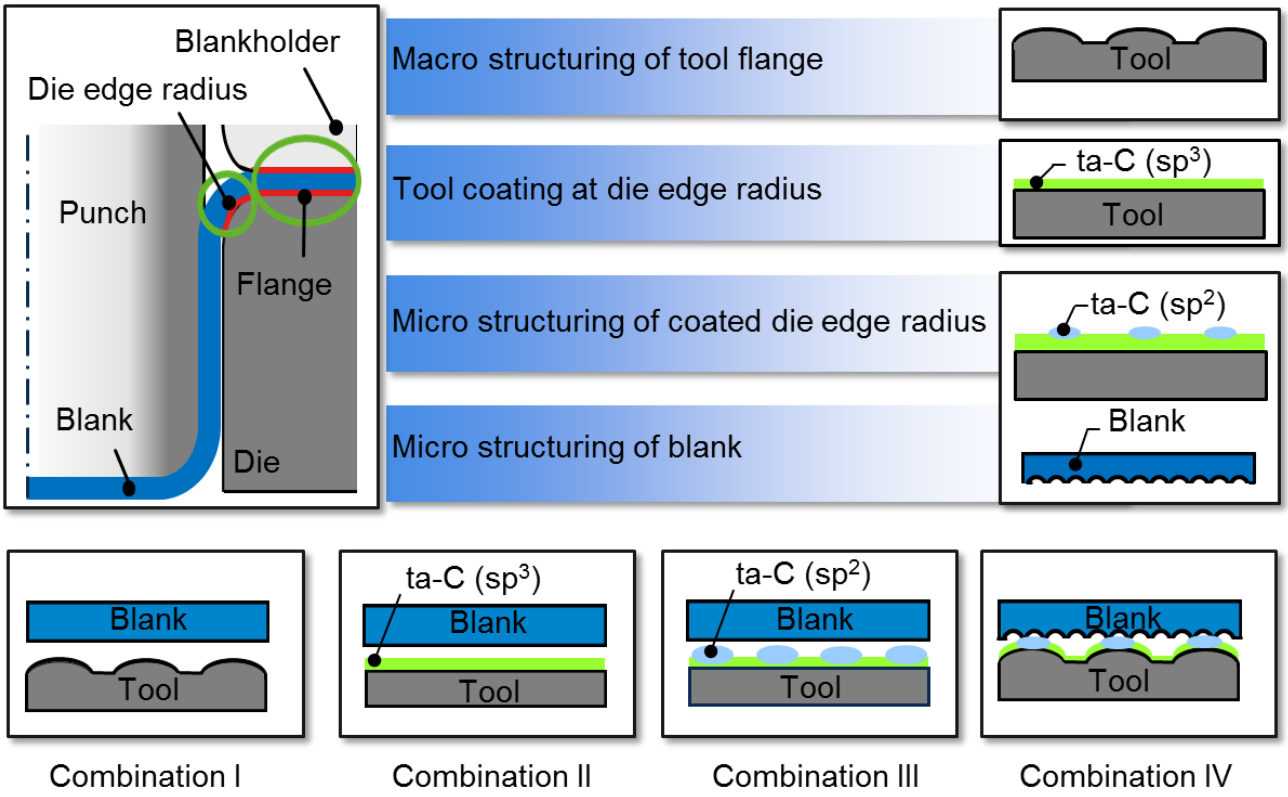

Fig. 1: Schematic representation of concept for lubricant-free deep drawing process: macro structures in the tool flange area demands an alternating bending of the blank in the drawing process; a protective tool-coating (ta-C) at the die edge radius reduces the friction coefficient and a subsequent micro structuring with Direct Laser Interference Patterning (DLIP) reducing the contact area; micro-structuring of the semi-finished products with a high-througput DLIP concept.

2 Preliminary work of macroscopic modifications

In the field of sheet metal forming, the deep drawing process is of greatest importance because of its versatility in process design. It is mostly used in large series production, such as in the automotive, household appliance

and packaging industries, but also in small and medium series production. Especially during deep drawing, frictional forces occur on large surfaces, which are additionally increased during the forming process. On the one hand the application of lubricant is particularly effective here. On the other hand this is most interesting in the sense of substitution by corresponding process developments due to its broad application. Therefore, in this proposed research project deep drawing with the aim of minimum quantity lubrication (or without additional lubrication) is investigated and corresponding process developments are proposed.

In deep drawing, the maximum drawing ratio is significantly influenced by friction. Too high friction forces between the workpiece, the blank holder and the die lead to bottom cracks. MEILER et al. [3] illustrated this clearly using the limit drawing ratio as a function of the friction coefficient as shown in Figure 2a. Forming limit lines 1 and 2 show failure by tearing, while the bottom line indicates the process limit by wrinkling. In addition, Figure 2b shows the situation in the process window. During deep drawing, the process window is limited by the occurrence of wrinkles and bottom cracks. By minimizing the lubricant, friction increases and therefore the required punching force increases. As a result, the risk of bottom cracks also increases. To ensure a larger or at least a constant process window, the effective friction, especially in the flange area, must be reduced. Especially smaller contact surfaces lead to a minimum frictional force in the sum. Therefore, the minimization of friction in the flange area of a deep drawing tool can be achieved by minimizing the tool surface in contact with the workpiece. In order to reduce the contact area between tool and sheet metal, the possibility of a macroscopic tool structuring was presented within the framework of this priority program. Macro structuring reduces the contact area to a line or point contact. However, this structuring increases the risk of wrinkling in the unsupported sheet metal areas, as the normally used blank holder force for stabilization is not applicable.

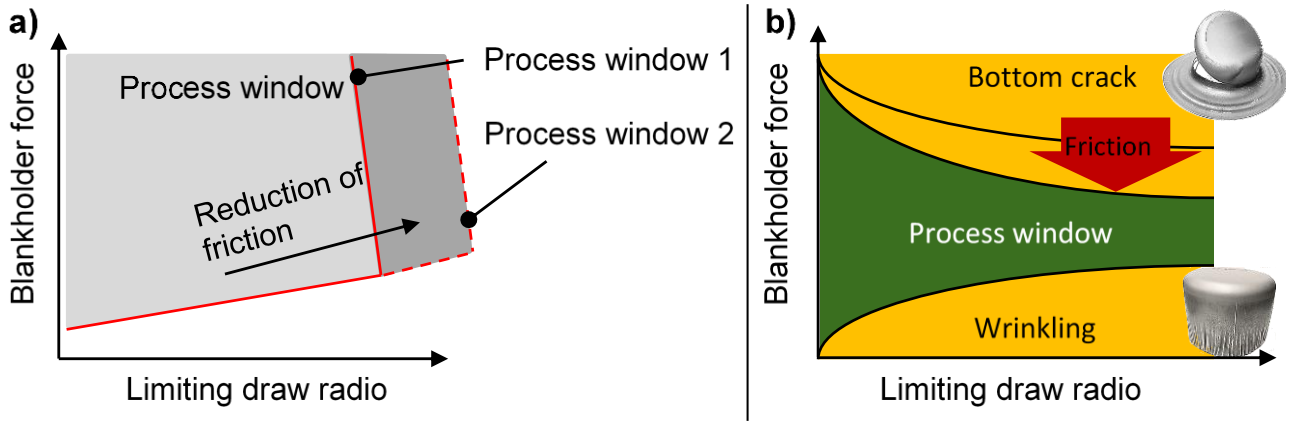

Fig. 2: a) Increasing process windows in deep drawing by reduction of friction based on [3], b) Reduction of process window, restricted by failure modes wrinkling and bottom crack

In order to ensure the stability of the sheet-metal in the non-supported areas against wrinkle formation, the macro-structured blank holder device is slightly immersed in the die. The induced alternating bending in the flange area increases the dent resistance of the semi-finished product in the tangential direction, which counteracts wrinkle formation and allows a significant reduction of the applied blank holder force (see Figure 3). The two positive effects of macro-structuring, namely the reduction of the contact area and the stabilization of the flange area, result in a sufficiently large and stable process window for the desired dry deep drawing process.

The combination of a small span λ with a high immersion depth δ has a positive effect on the avoidance of wrinkling in the flange by increasing the moment of inertia of the surface, but at the same time increases the necessary drawing force and thus the risk of bottom tearing. A large support span λ with a low immersion depth δ reduces the drawing force and reduces the risk of bottom cracks but increases the probability of wrinkling. For a stable process, it is therefore essential to identify suitable parameters for support span λ, immersion depth δ and the resulting curvature.

For a time-efficient determination of these parameters with interdepending variables, a semi-analytical model for process modelling and prognosis of the process window regarding wrinkling and bottom cracks was developed within the framework of this project. The model was initially based on the special case of axis-symmetric deep drawing and was adapted for an application to non-rotationally symmetrical components.

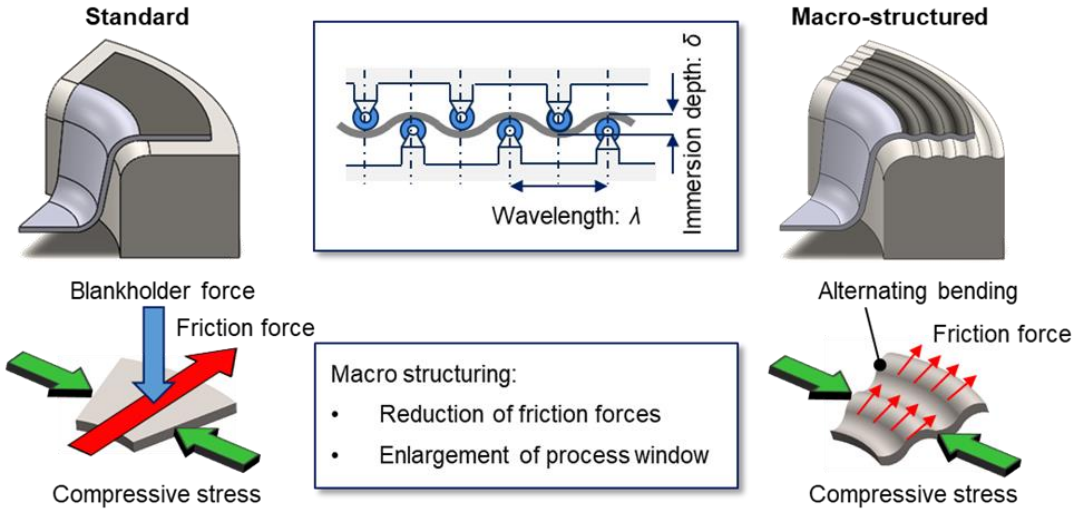

Fig. 3: Macro structuring of deep drawing tool: reduction of friction forces and avoiding wrinkling by reducing the contact area in the flange area of deep drawing tools, from the standard tool setup to the macro structured tool setup for lubricant free deep drawing processes.

2.1 Process modelling: Determination of process window

The process modelling for the design of the macro-structuring must consider the two relevant failure cases in the deep drawing process, which represent the limits of the usable process window. On the one hand, this is the occurrence of bottom cracks when the permissible maximum punch force is exceeded, and on the other hand, the formation of wrinkles in the flange. For the determination of the occurring punch force, a detailed energy calculation was developed and carried out, while an analytical buckling analysis was used for the prediction of the wrinkle formation.

In order to be able to predict bottom cracks during deep drawing with macro-structured tools, the drawing force must be compared with the permissible maximum drawing force as a result from the material strength. The prediction of the acting drawing force is based on an energy equilibrium. The energy coming from integrating the punch force over the punch displaement has to be the same like the required total inner energy, which is composed of the ideal forming energy, the bending energy at the drawing edge rounding and the alternating bending in the flange, as well as the energy due to friction. The calculation of the actual drawing force is carried out using the approaches for conventional deep drawing according to DOEGE and LANGE [4, 5], which will be extended and adapted accordingly for the new process with macro-structuring. The total energy required for conventional deep drawing, which is composed of the ideal forming energy E_{Ideal}, the bending energy at the drawing edge radius E_{Bending} and the energy to overcome friction E_{Friction}, must be taken into account with macro-structured tools for deep drawing, a further energy component that considers the alternating bending in the flange area, as shown in Figure 4.

$$\mathrm{E_{Total}} = \mathrm{E_{Total}} + \mathrm{E_{Bending}} + \mathrm{E_{Friction}} \quad \text{(Eq. 1)}$$

$$\mathrm{E_{Total}} = \int_0^h \mathrm{F}_{Punch} \cdot \mathrm{d}h \quad \text{(Eq. 2)}$$

$$\mathrm{E_{Ideal}} = \sqrt{\frac{\bar{r}+1}{\bar{r}+\frac{1}{2}}} \cdot \delta \mathrm{V_{Formed}} \cdot \delta \mathrm{h} \cdot \int_{\mathrm{r_i}}^{\mathrm{r_a}} \mathrm{a} \left[\frac{2}{\sqrt{3}} \ln \left(\frac{\sqrt{\mathrm{R_0^2 - R_a^2 + r^2}}}{\mathrm{r}} \right) \right]^{\mathrm{n}} \cdot \frac{1}{\mathrm{r}} \mathrm{dr} \quad \text{[Dog04, Lenz82]} \quad \text{(Eq. 3)}$$

$$\mathrm{E_{Bending}} = \left(\mathrm{r_m} + \frac{\mathrm{s}}{2} \right) \cdot \sqrt{\frac{\bar{r}+1}{\bar{r}+\frac{1}{2}}} \cdot \delta \mathrm{V_{Formed}} \cdot \delta \mathrm{h} \cdot \int_0^{\beta} \frac{\cos(\beta)}{\mathrm{r}(\beta)} \cdot \mathrm{k_f}(\beta) \mathrm{d}\beta \quad \text{[Dog04]} \quad \text{(Eq. 4)}$$

$$\mathrm{E_{Friction}} = \frac{\mu}{(\mu - 1)} \cdot \sqrt{\frac{\bar{r}+1}{\bar{r}+\frac{1}{2}}} \cdot \delta \mathrm{V_{Formed}} \cdot \delta \mathrm{h} \cdot \left(\left(\frac{1}{2} \beta + \frac{1}{\mu - 1} \right) \cdot \mathrm{k_{f,1}} + \beta \cdot \mathrm{k_{f,2}} \right) \quad \text{[Dog04]} \quad \text{(Eq. 5)}$$

with: $\bar{r}$: Mean perpendicular anisotropy, $\delta V_{\mathrm{formed}}$: Forming volume, δh: Virtual punch displacement, h: Punch displacement, a, n: Material constants, R_0: Initial radius of sheet metal, R_{a}: Current radius of flange, r: Radius coordinate of material point, r_{m}: Bending radius, β: Bending angle, s: Sheet thickness, μ: Friction coefficient, $k_{\mathrm{f,1}}, k_{\mathrm{f,2}}$: Yield stress before and after bending and F_{Punch}: Punch force.

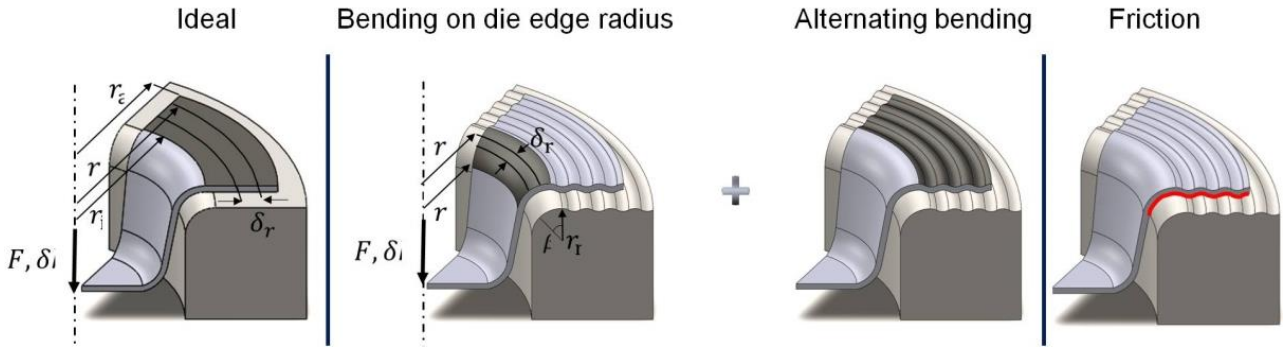

Fig. 4: Calculation of energy parts for deep drawing with macro-structured tools.

Here, n is the number of alternating bends of the sheet metal, and E_{WB}, the energy required for alternating bending, taking into account the strain hardening in the flange area. The energy components are calculated by combining the models of DOEGE ET AL [4] and LENZE [6] using the "principle of virtual work". It is assumed that the work due to a "virtual displacement" at the inner edge of the flange is equal to the work due to "virtual displacements" in the flange volume and that volume constancy exists at constant sheet thickness. The individual energy components were calculated as shown in Figure 4.

The model for calculating the alternating bending as well as the bending at the drawing edge radius was adapted for macro-structuring in the flange area by using corresponding input parameters such as bending radius r_m, bending angle β and position of the bend $r(\beta)$. The calculation of the integrals was numerically done using the trapezoidal rule. The incremental process consideration allows the process time and the relevant non-linearities to be taken into account. The actual drawing force can be calculated using the derived energy equation. This is compared with the maximum permissible stamping force, which is defined by the tensile strength of the material and the present sheet metal cross section. In this context it should be noted that the maximum possible transferable punch force is limited by the effective sheet thickness at the transition between bottom edge and side wall. DOEGE has shown that the measured maximum drawing force at rupture F_{BR} can be up to a factor of 1.55 greater than the calculated force F_{BR}. This difference can be recorded as a correction factor by the so-called dimensionless tear factor α_R [7].

In order to determine this factor analytically, it must be assumed that neither the bending nor the tangential compressive stress and the appearance of sliding in the area of the punch edge as well as any friction above the punch edge rounding influence the transmissible force. It remains to be expected, however, that the punch edge radius, the sheet thickness, the drawing ratio and the effective stress condition will influence the tear factor. This relationship can be derived by including the natural exponential function. The process can be considered stable with regard to bottom cracks if the present punch force is smaller than the bottom crack force ($F_{st} < F_{BR}$). The analytical model presented here has been verified by experimental tests, as shown in Figure 5. For the deep drawing of sheet metal from DC04 with a diameter of D_0 = 180 mm and a sheet thickness of 0.6 mm and 1.0 mm, the analytically calculated and experimentally measured punch force for the considered immersion depths of δ = 0.2 mm and 0.4 mm in all variants is below the critical bottom tensile force calculated from the uniaxial tensile test, see Figure 5 left.

As expected according to the analysis, no bottom cracks occurred in the experiments. For a diameter of D_0 = 200 mm and a sheet thickness of 0.6 mm, the analytical observation predicted the occurrence of bottom cracks at an immersion depth of δ = 0.4 mm, which was confirmed in the tests carried out. For the other variants with an immersion depth of δ = 0.2 mm or a higher plate thickness of 1.0 mm, the analytical analysis did not indicate any failure, which was also shown in the experimental results. In sum, the results show that the implemented approach is suitable for the fast prediction of the occurrence of bottom cracks.

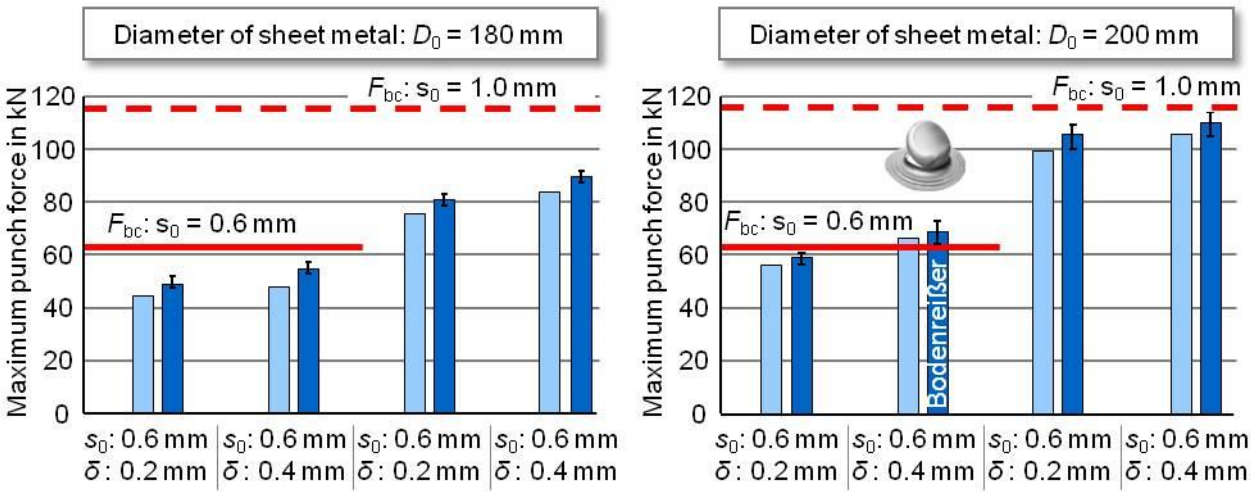

Fig. 5: Verification of the developed model and criterion for predicting the bottom crack, for sheet metal diameters of 180 mm and 200 mm.

2.2 Process modelling: Determination of wrinkling

In order to be able to make a statement about the generation of wrinkles during deep drawing with macro-structured tools, the stability of the sheet must be examined with regard to the stress state present in the flange. In general, the axissymmetric areas with the highest tangential compressive stresses (cause of wrinkling) and the lowest radial tensile stresses (stabilizer) are considered (element 1, Figure 6), as the risk of wrinkling is greatest in these areas. In addition, deep drawing with macro-structured tools is a special case in that the edge area of the flange (red zone), in contrast to the inner areas (element 2, Figure 6), is supported by the tool on one side only and forms a free end. This free end is therefore the critical area to be considered for the occurence of wrinkles and is examined within the framework of a stability analysis to determine the critical tangential stresses. Because the critical area is a free sheet metal end, it is modeled for the buckling analysis as a one-sided rectangular plate with width a and length b, which is compressed with $\sigma_t(r)$ and drawn with $\sigma_r(r)$. Considering the equilibrium of forces, the tangential and radial stress acting on the free end can be calculated as follows as a function of the workpiece radius using the TRESCA flow condition.

$$\sigma_r(r) = k_f(r) \cdot ln\left(\frac{r_0}{r}\right) \quad \text{(Eq. 6)}$$

$$\sigma_t(r) = \sigma_r(r) - k_f(r) \quad \text{(Eq. 7)}$$

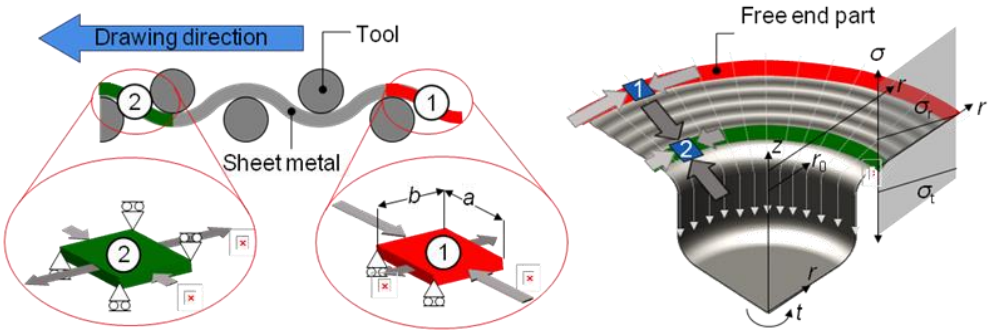

Fig. 6: Assumption done for modelling the buckling effect in deep drawing, area 1 is more critical with respect to buckling than area 2 due to free, unsupported end in area 1. Therefore, modelling of buckling is limited to area 1 as weakest area in the whole part geometry.

Because the free end is supported on one side and freely movable on the other, the balance of forces can be described by equation 8. The deflection w of the element in z-direction as a function of element dimensions and number of occurring sine waves (wrinkles) is calculated by equation 9. For the required prediction of this number of wrinkles, SENIJOR has developed a model for deep drawing without hold-down in [8] using energy methods (equation 10). Von KÁRAMAN has shown in [9] that the conventional elastic bending theory can be extended to calculate plastic bending by substituting young's modulus E with the modulus for plastic buckling

E_0 (equation 11). Taking into account the boundary conditions and the dimensions of the free end, the critical tangential stress $\sigma_{t,cr}$ can be determined by solving equations 8 to 11, as described by equation 12.

$$\frac{\partial^4 w}{\partial x^4} + \frac{2\partial^4 w}{\partial x^2 \partial x^2} + \frac{\partial^4 w}{\partial y^4} = \frac{12(1-\nu^2)}{E s_0^3}\left(\sigma_t \frac{\partial^2 w}{\partial x^2} - \sigma_r \frac{\partial^2 w}{\partial y^2}\right) \quad \text{(Eq. 8)}$$

$$w = \sum_{m=1,2,3,\ldots} \sum_{n=1,2,3,\ldots} w_{mn} \sin\frac{m\pi x}{a} \sin\frac{n\pi y}{b} \quad \text{(Eq. 9)}$$

$$1.65\frac{r_m}{r_0 - r_i} \le m \le 2.33\frac{r_m}{r_0 - r_i} \quad \text{(Eq. 10)}$$

$$E_0 = \frac{4EP}{\left(\sqrt{E}+\sqrt{P}\right)^2} \quad \text{(Eq. 11)}$$

$$\sigma_{t,\,Kr} = \frac{\pi^2 E {s_0}^2 \left(\left(\frac{m}{a}\right)^2 + \left(\frac{1}{b}\right)^2\right)^2}{12(1-\nu^2)\left(\left(\frac{m}{a}\right)^2 - \left(\frac{\sigma_r}{\sigma_t}\right)\left(\frac{1}{b}\right)^2\right)} \quad \text{(Eq. 12)}$$

a:Perimeter of free end of geometry
b: width of free end of geometry
w: buckling amplitude in z-direction
ν: Poisson's ratio
E: Youngs modulus
m: Number of wrinkles
r_m: mean flange radius
r_0: Initial radius of sheet metal
r_i: Inner flange radius
E_0: Effective youngs modulus for plastic buckling
P: Tangent modulus
$\sigma_{t,kr}$: critical tangential stress

Experimental investigations have been carried out to verify the calculations for critical tangential stress. For this purpose, DC04 sheets with three different thicknesses (s_0 = 0.3 mm, 0.5 mm and 0.6 mm) and a diameter of D_0 = 200 mm were selected for deep drawing with macro-structured tools with an immersion depth of δ = 0.2 mm. Figure 7 shows the tangential stress curve during deep drawing and the critical tangential stresses for the three sheet thicknesses.

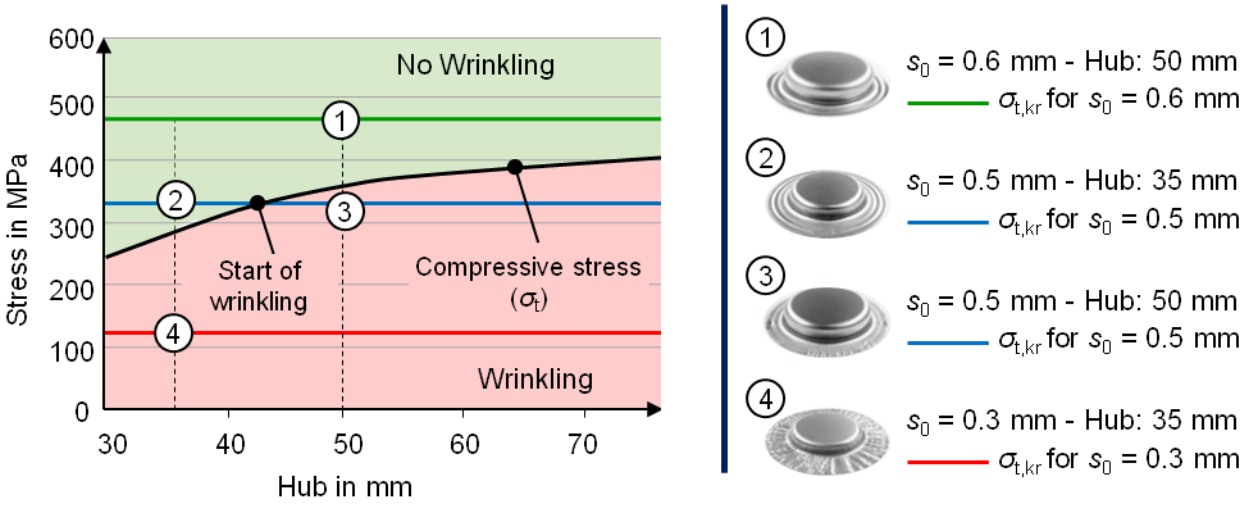

Fig. 7: Critical tangential stresses during deep drawing for different sheet thicknesses (s_0 = 0.3 mm, 0.5 mm and 0.6 mm) and a diameter of D_0 = 200 mm. The immersion depth δ was 0.2 mm.

Figure 7 shows that the tangential stress (σ_t) for deep drawing the sheet with s_0 = 0.6 mm always remains below the calculated critical tangential stress ($\sigma_{t,cr}$). Therefore no wrinkling is to be expected here (component 1). In contrast, σ_t for deep drawing of the sheet metal with s_0 = 0.3 mm is far above $\sigma_{t,cr}$, so that a very early wrinkle formation in the process can be expected (component 4). The results show that with a thickness of s_0 = 0.5 mm and a stroke of h_1 = 35 mm σ_t is below $\sigma_{t,cr}$ and no wrinkling is to be expected (component 2). When the punch displacement reaches h_2 = 45 mm, σ_t exceeds the critical value $\sigma_{t,cr}$ and wrinkling is expected to begin, as can also be seen on component 3 at the edge of the flange. The experimental results show a good agreement with the expectations from the stability analysis.

The transferability of the analytical model to non-rotationally symmetric components has been demonstrated using rectangular tools from 1.2379. For theoretical consideration, the rectangular cup can be divided into four axissymmetric corners and four non-curved segments. Since there is no tangential compressive stress in the straight regions, the ideal forming energy is not considered here.

Figure 8 shows that the results from the analytical model also correspond very well with the FE analyses and the real experiments. The calculated energies can be used in an analogous way for the evaluation of the developed criteria for a detection of bottom cracks and for the evaluation of the increased probability.

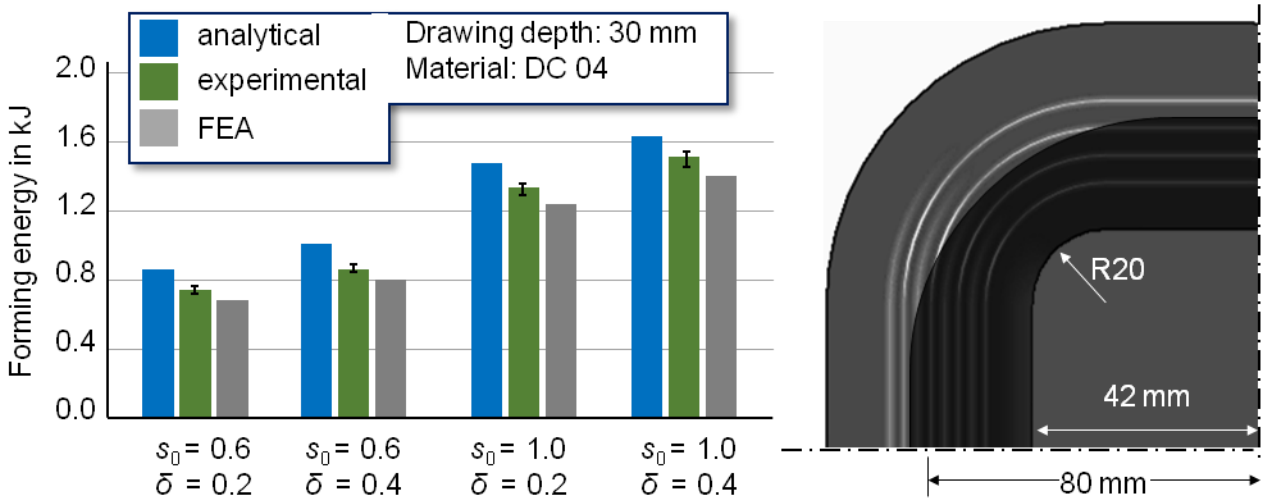

Fig. 8: Comparison between analytical, experimental and FE results for calculating the forming energy of a rectangular cup.

The transferability of the model equations to non-axissymmetrical geometries was verified by means of an investigation of the process window borders (wrinkle formation and bottom cracks). On the basis of the analytical equations, the formation of bottom cracks by maximizing the immersion depth and the formation of wrinkles by minimizing them, respectively, was specifically enforced. Figure 9 shows exemplary results for a stable and an unstable process for axissymmetric and non-axissymmetric components made of DC04 with a constant span of the macro-structuring of the tool from λ = 8.0 mm.

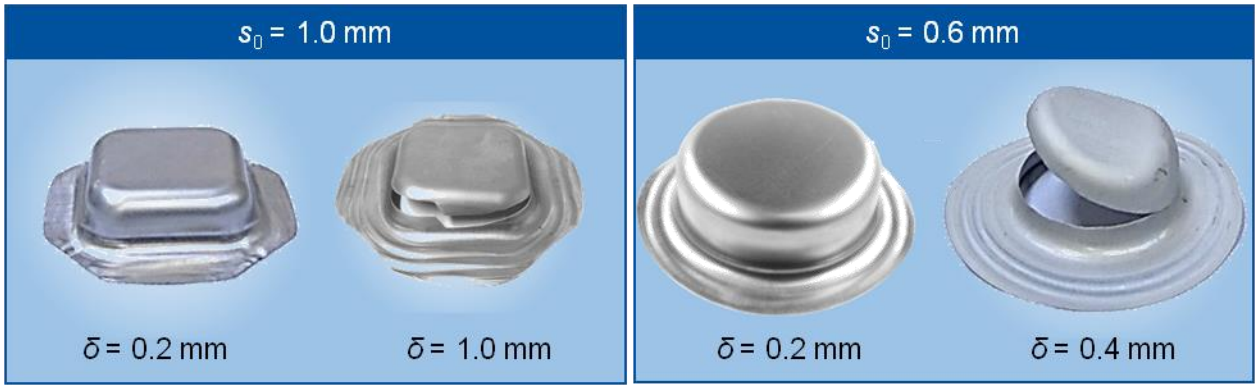

Fig. 9: Feasibility study of deep drawing with macro-structured tools

2.3 Application of macro-structuring to high strength sheet materials

Within the second funding period, dry deep drawing with high-strength materials and increased sheet thicknesses was carried out as an example in order to analyze the process limits of the process with regard to dry deep drawing. For this purpose, tests were carried out with a hot-dip galvanized complex-phase steel (HDT780C) with a yield strength $R_{p0.2}$ of 780 MPa, a ultimate tensile strength R_m of 820 MPa and an initial sheet thickness s_0 of 2.0 mm. The blanks with different diameters between 160 mm and 200 mm were deep drawn with both macro-structured and unstructured standard tools. As Figure 10 shows, the measured punch force for the macro-structured tool always below the punch force of the standard tool.

The blanks with a diameter of 190 mm have been deep drawn both with the standard dry and lubricated tool (with the WISURA ZO3368 provided for benchmark purposes) and with the non-lubricated but macro-structured tool. The drawing force for deep drawing with the macro-structured tool is even lower than with the standard tool in lubricated condition. Furthermore, the blanks with a diameter of 200 mm cannot be deep drawn

to the end of the process with either a dry or lubricated standard tool. However, this is possible with the macro-structured tool and proves the extension of the process window for deep drawing by the macro-structuring of the tools.

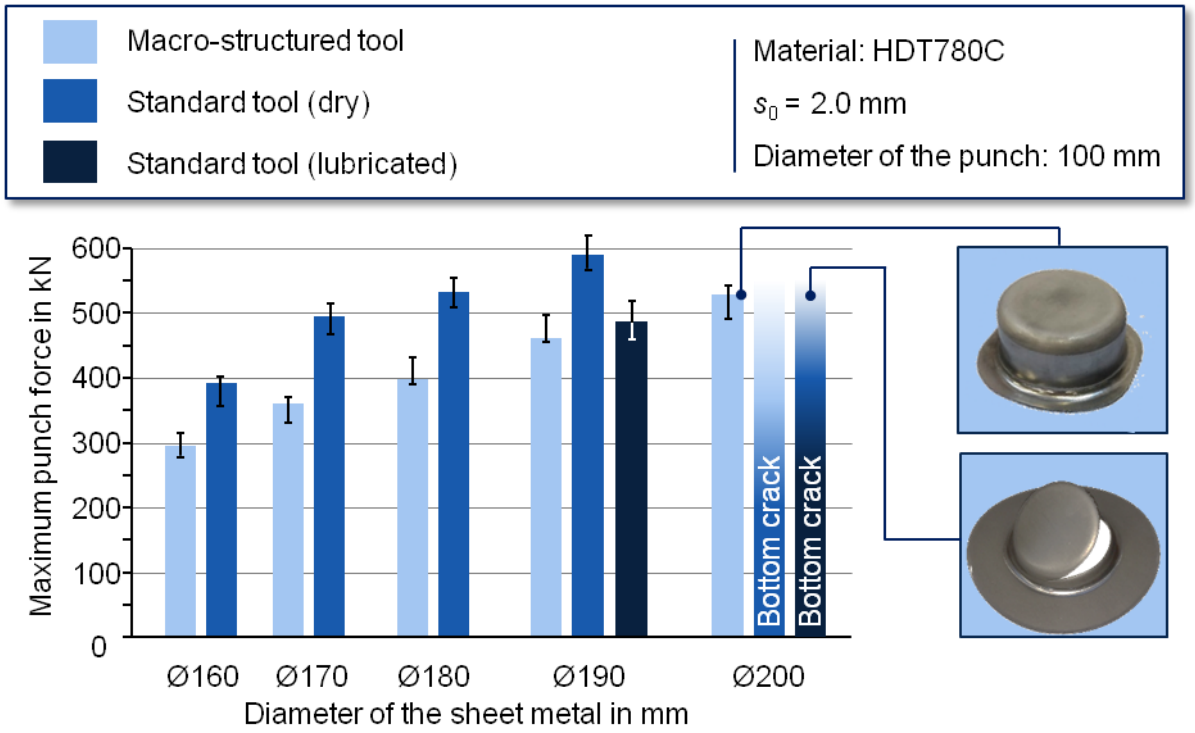

Fig. 10: Applicability of macro-structured dry deep drawing with high strength materials

2.4 Alternating bending to adjust the properties of components

One challenge of sheet metal forming processes is always the elastic springback of components. This phenomenon is highly dependent on the material, in particular its hardening behavior, the sheet thickness, the part geometry and the forming history. One aim of macro-structured deep drawing is to set up a robust process with regard to feasibility and shape and dimensional accuracy, i.e. the safe placement of the working point in the process window. For this purpose, the influence of the kinematic hardening of the material by the macro-structuring with regard to the springback behavior is to be eliminated as far as possible. Since the material is subjected to multiple plastic alternating bending during deep drawing with macro-structured tools, a possible BAUSCHINGER effect, caused by the property of kinematic hardening of the material, can have a great influence on the resulting springback. Since this material property cannot be influenced, the robustness of the dry deep-drawing process should be improved by eliminating this material property from having a significant influence on the dry deep-drawing result.

In the first investigation, the influence of kinematic hardening on the springback behavior of components by forming a cap profile was examined. For this purpose the macro-structured tool with a constant span of 8.0 mm was used. The springback of the three materials DC04, AA5182 and DP600 in two extreme cases, i.e. materials with 100% isotropic hardening and 100% kinematic hardening, was simulated with the help of FEM and the results were compared with experimental tests for two different immersion depths of 0.0 and 0.2 mm. The numerical results based on the FEM simulation for the drawing of hat profiles with macro-structured tools show that the restraining force caused by alternating bending in the flange area compensates the springback of the workpiece independent of the type of hardening, as shown in Figure 11.

As it can be seen, springback is reduced by generating alternating bending for all types of hardening in all test materials. The results show that alternating bending can reduce springback of materials with pure isotropic hardening behavior more than materials with pure kinematic hardening behavior. Since springback is a function of the yield strength, the material strength during alternating bending can slightly influence the springback

of materials with predominant kinematic hardening behavior. However, experimental and numerical results show that, taking into account these opposite effects, the restraining force has a major influence on the springback behavior of materials. In order to investigate the influence of alternating bending on the dimensional accuracy of closed components, the ring splitting method was investigated within the framework of the priority program. For this purpose, a ring was cut from the frame area of the rotationally symmetrical cups and then the ring was disassembled. The opening gap in the ring can show the large springback in the rim area of the cup. The investigations were carried out with DC04 and Al 5182. The macro-structured tool has a constant wavelength of λ = 8.0 mm. The sheets of DC04 and Al5182 with an initial diameter of D_0 = 180 mm and a thickness of s_0 = 1.0 mm were cleaned with a citrus-based cleaner and finally treated with acetone to remove the pre-lubricant and ensure a comparable test condition. The samples, which would have to be deep-drawn with standard tools, were lubricated with lubricant "WISURA ZO 3368". The deep-drawn parts were cut by an electrical discharge process to prevent the external residual stresses caused by the cutting process.

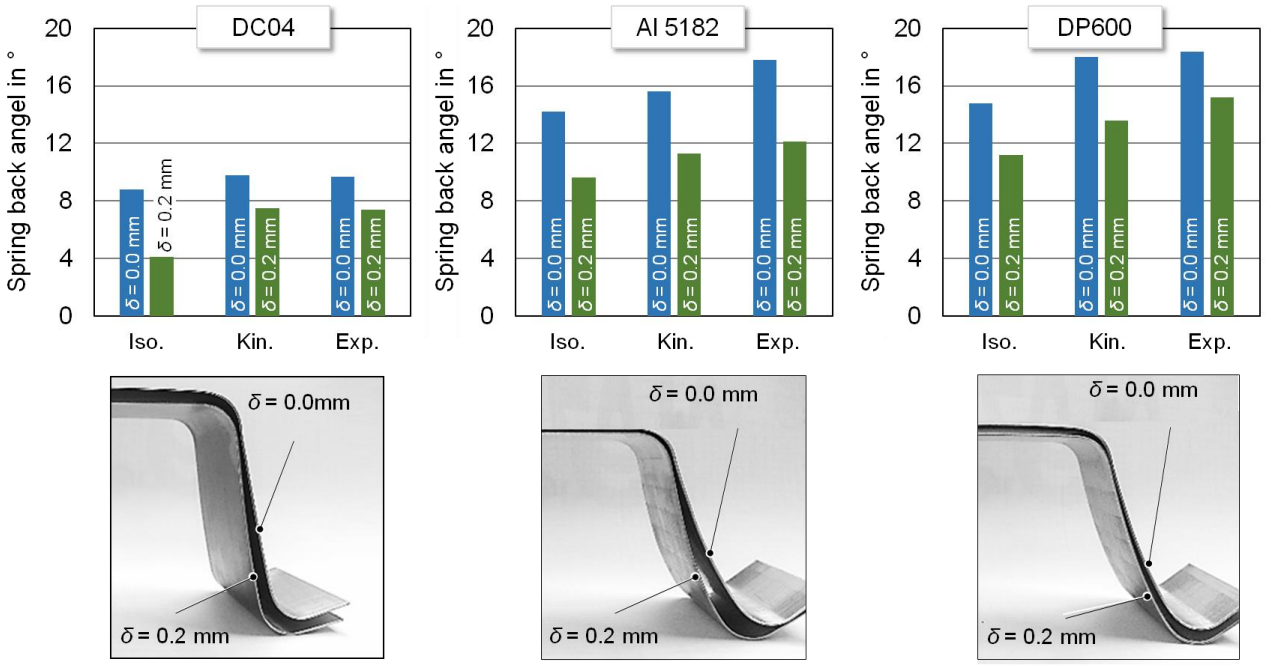

Fig. 11: Springback reduction as a dependency of immersion depth δ in a drawn U-profile, with increasing immersion depth the alternating bending effect will be increased as well as the restraining force; due to that stretching of the flange area, the spreingback effect is reduced.

The results show that by increasing the immersion depth in the macro-structured deep-drawing process, springback can be reduced. Furthermore, the induced alternating bending in the newly developed process leads to a compensation of the springback of the component by the induced restraining force due to alternating bending as well as the further elastic-plastic deformation of the material during the alternating bending mechanism. Table 1 and Figure 12 shows an overview of the rings after splitting.

2.5 Transfer to non axis-symmetric geometries

In order to verify the lubricant-free deep drawing process under practice-relevant conditions, both standard and macro-structured tools for deep drawing a T-cup due to its complex stress state in the flange area were designed and manufactured within the framework of the completed priority program 1676. The two criteria for predicting the process limits were applied to the tool design. Based on this, no bottom cracks and no wrinkling were expected, which was experimentally confirmed. Furthermore, the results showed that the maximum punch force during deep drawing with macro-structured tool under lubricant-free conditions is only marginally higher than that during conventional deep drawing with spacer ring using lubricant. Furthermore, the results showed that conventional deep drawing without the use of lubricant caused the sheet metal rupture due to the applied blank holder force. However, the use of a spacer ring in conventional deep drawing under lubricant-free conditions also resulted in a stable process without any significant difference in punch force compared to deep drawing with macro-structured tools. However, in the latter process, due to its ability to control the flow of material during the process, no dent in the bottom area of the part occurs.

Table 1: Result of ring splitting test.

Material	Opening gap in mm		
	Standard	δ = 0.2 mm	δ = 0.4 mm
DC04	50	45	37
AA 5182	95	73	64

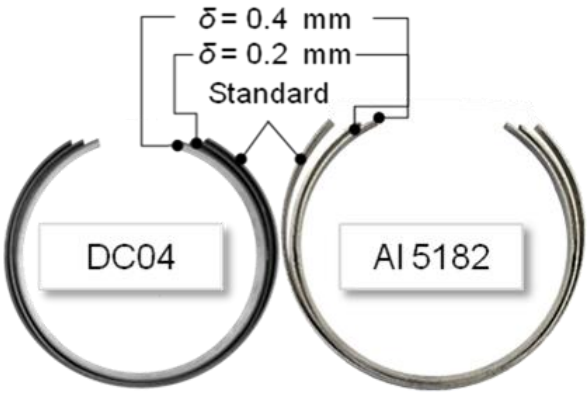

Fig. 12: Influence of immersion depth on springback behavior (for Opening gap δ = 0.4 mm and 0.2 mm). Materials: DC04 and Al5182.

In addition, the results displayed in Figure 13, showed that the maximum punch force in deep drawing with a macro-structured tool under lubricant-free conditions is only marginally higher than that in conventional deep drawing with a spacer ring using lubricant. Furthermore, it was shown that conventional deep drawing without the use of lubricant came to the bottom tear due to the applied blank holder force. However, the use of a spacer ring in conventional deep drawing under lubricant-free conditions also resulted in a stable process without any significant difference in punch force compared to deep drawing with macro-structured tools. Nevertheless, in the latter process, due to its ability to control the flow of material during the process, no dent in the bottom area of the part occurs.

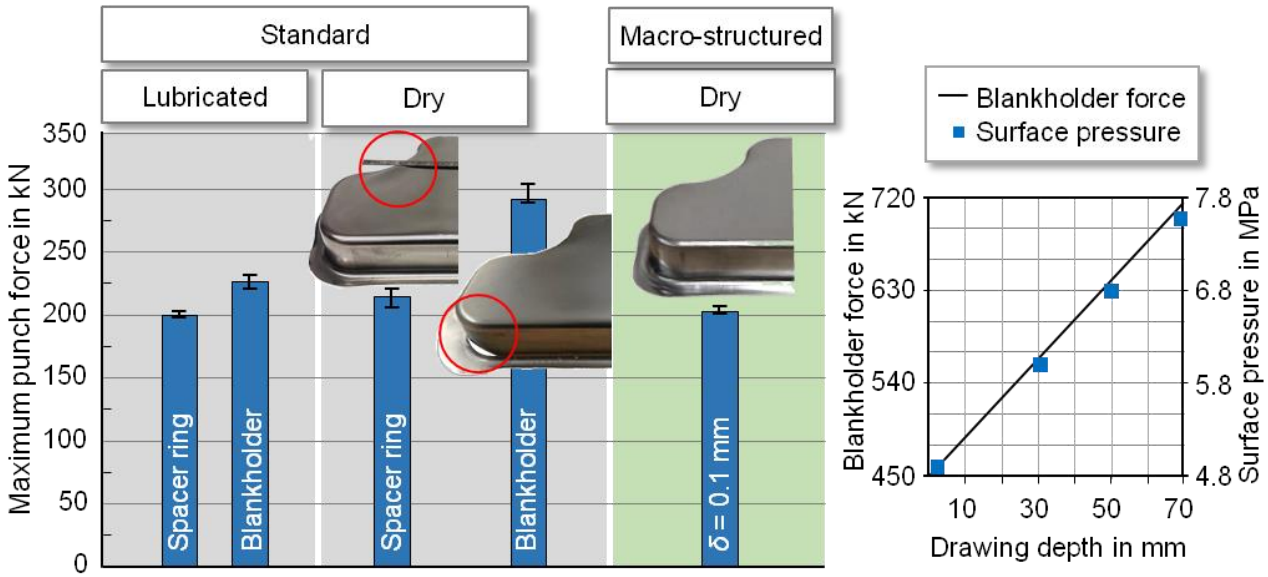

Fig. 13: Transfer of results on complex 3D-part; Reduction of maximum punch force my macro-structuring of tool surface despite the absence of lubrication (left); usually critical increasing blankholder force as a function of the drawn depth during deep drawing as a result of using a spacer ring – here without any negative influence on the result due to macro-structuring (right)

3 Development of a load-compatible layer system

Within the framework of the sub-project "Development of a load-compatible coating system for deep-drawing tools", highly wear-resistant tetrahedrally bonded amorphous carbon layers (ta-C) were deposited using the pulsed vacuum arc (short pulsed Arc - spARC) technique. In contrast to alternative deposition processes for ta-C coatings, the Arc processes are characterized by the fact that it can deposit ta-C coatings using relatively inexpensive PVD equipment at high coating rates (up to 1 - 2 µm/hour) [10]. A disadvantage here can be the large defect densities in the coating which arise simultaneously [11]. Furthermore, residual stresses in the coating can influence the adhesion of the coating, which has a considerable influence on the service life or general usability of thicker coatings [12]. A PVD coating system from Oerlikon (see Figures 14a and 14b) as well as Innovap (see Figures 14c and 14d) was used in the tests. In particular, tests on doped layers were carried out with the Inovap system, whiletests on smoothed layers were mainly carried out on the Oerlikon system.

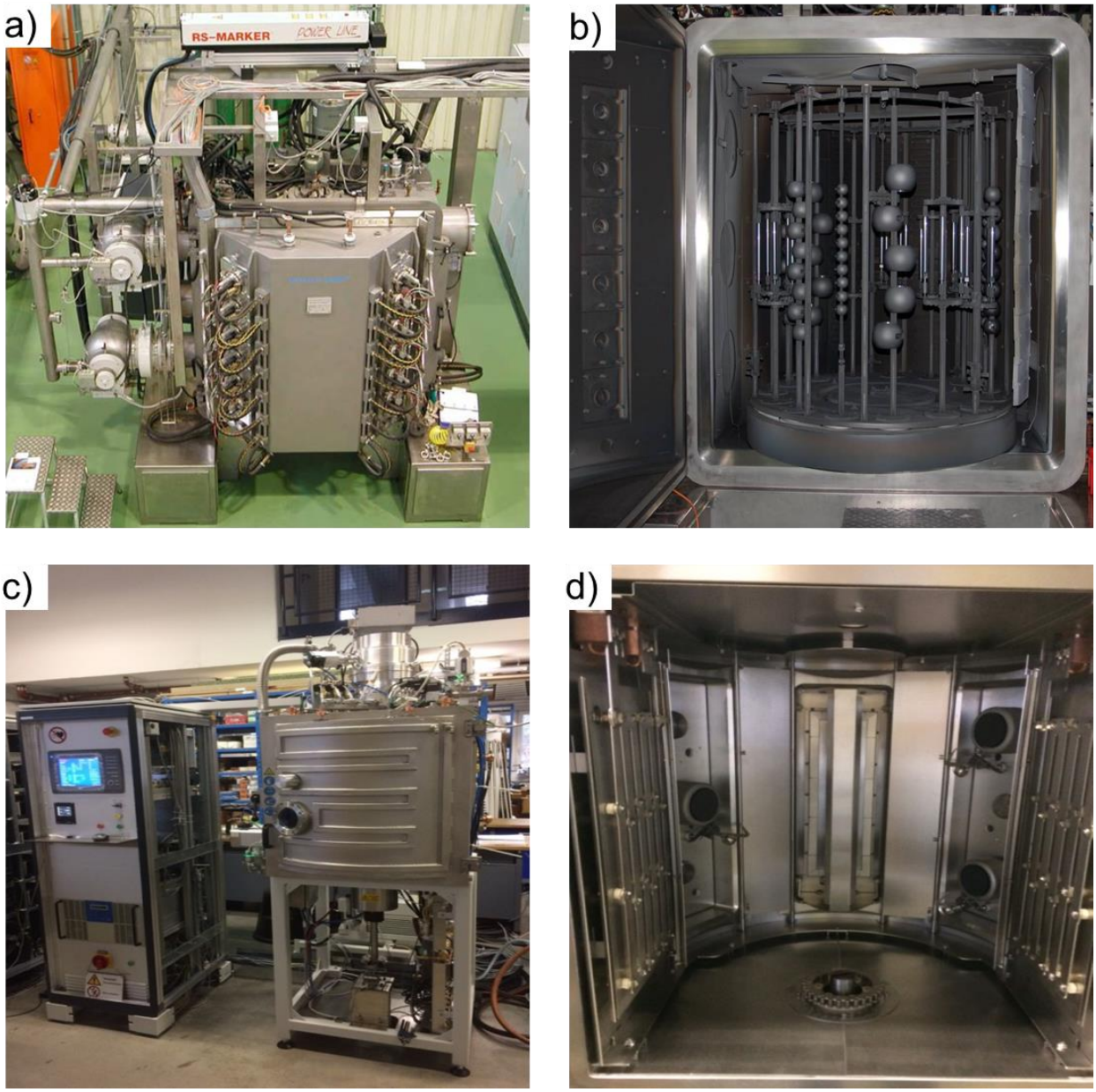

Fig. 14: a) and b) Oerlikon system with a chamber size of 1 m height and 1 m diameter. c) and d) system of the company Inovap for the deposition of doped layers.

The spARC® is a combination of a direct current (DC) vacuum arc (a process widely used in industry for the deposition of wear protection layers) and short high current pulses. These current pulses cause an increase in the energy and ionization rate of the layer-forming carbon ions, which results in a high diamond bond content

in the layer. Very hard layers with hardnesses of up to 75 GPa can be deposited [13]. Advantageous applications of these coatings are therefore, for example, tools for the mechanical processing of metals such as aluminium, copper, brass or even CFRP, where they reduce tool wear and the formation of built-up edges.

Within the scope of this project, the application for the processing of steel samples in forming tests was investigated. The coating of formed parts is particularly advantageous where, as addressed within this priority program, lubricants are not used due to environmental aspects.

Within the project, the process parameters shown in Table 2 were used for the deposition of ta-C coatings.

Table 2: Representation of the essential process parameters for the deposition of ta-C coatings using spARC technology. Furthermore, characteristic properties of ta-C coatings deposited by spARC-technique.

Technical data for the production of ta-C using spARC technology	
Arc current	100 A
Pulsed arc current	1600 A
Pulse length	0.25 ms
Pulse frequency	100 Hz
Deposition rate	1.6 µm/h
Coating duration	160 min
Pressure during coating	10^{-5} mbar
Deposition temperature	< 150 °C

Technical data of ta-C	
Hardness	21 - 45 GPa
E-Modulus	360 - 450 GPa
Friction coefficient (dry, polished, after Strip tensile bending test)	~0.13 – 0.18
Coating thickness	1.6 – 3.5 µm
Temperature stability	350 °C

3.1 Surface roughness and layer characterization

The main development goal within the first half of this subproject was to reduce the surface roughness of the coated components and to identify important influencing parameters, as these have a significant influence on the tribological properties. Essential influencing factors are:

a) component wear, that formed material is deposited at roughness peaks of the tools;

b) the coefficient of friction between tribological partners can be increased to an adverse extent;

c) the running-in behaviour of the tribological system is prolonged until the roughness is smoothed out and

d) the influence of surface structuring is eliminated.

For this reason, the development of roughness in relation to the material used (1.2379) was examined in detail and compared with the roughness development of alternative steel materials (1.4301, 1.3505 and 1.3343). For this purpose, the roughness was measured by means of the tactile step method. Within these investigations, the roughness development and reduction both during and after the coating process was examined in order to show ways in which the resulting layer roughness can be reduced most effectively.

The evolution of surface roughness has been investigated at different stages of the coating process. As shown in, different working steels and a stainless steel have been compared with respect to their polishability and the resulting roughness (see Figure 15a). The surface pretreatment was carried out using both polishing pastes (diamond suspension 1 µm and 3 µm particle size) and abrasive paper (grain size: 500, 1000, 4000). It is characteristic that the softer comparison material 1.4301 in particular shows higher roughness with abrasive paper with a coarse grain size. The actual coating process is preceded by a metal ion sputtering process to remove water and impurities from the surfaces and thus to achieve an adhesive bond between the surfaces.

After metal ion sputtering, rolling bearing steel 1.3505 and 1.3343 in particular showed higher roughness with increasing process duration (see Figure 15b). The steel 1.2379 used within the project, on the other hand,

showed lower increases in Ra roughness after metal ion sputtering compared to the materials 1.3505 and 1.3343. Since metal ion sputtering simultaneously heats up the samples, it is advantageous to choose this process for a short time, as otherwise the process times can be considerably longer. It is also advantageous to further classify material-related process parameters in order to reduce or optimize the coating time.

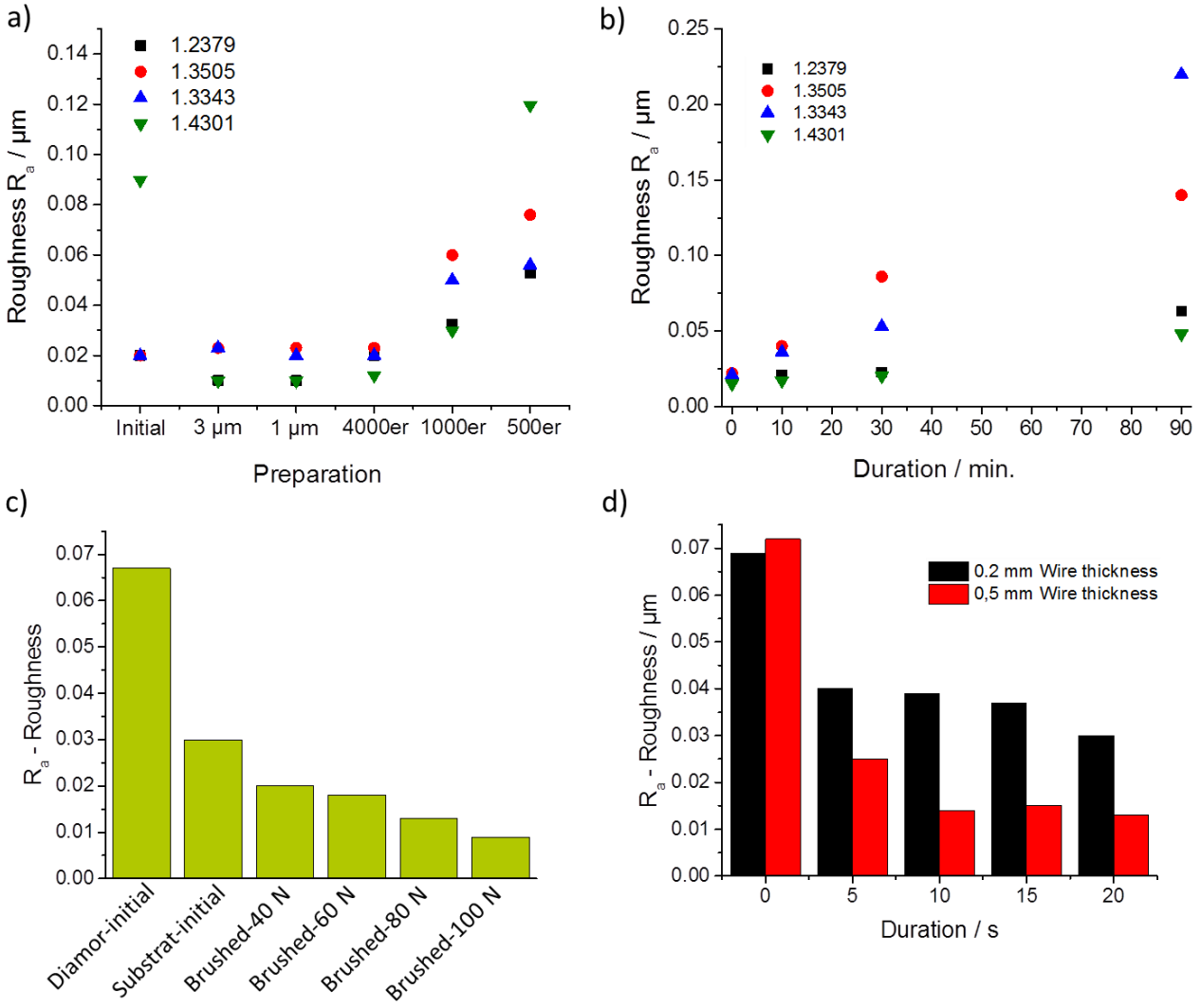

Fig. 15: Ra values as a function of a) sample pretreatment and b) process time for metal ion sputtering of 1,2379 compared to other steels. Ra values of an approx. 1 µm thick ta-C layer as a function of c) the normal force when brushing the sample (processing time 50 s, wire thickness 0.2 mm) and b) the processing time of the brushing (wire thickness 0.2 mm, normal force 60 N).

In addition, these results show that the subsequent coating contributes to a significant extent to the increase in layer roughness (e.g. Ra = ~0.07 µm for a 3.0 µm thick layer). Subsequent polishing of the layers with a wire brush is therefore necessary for unfiltered ta-C layers in order to smooth in or remove the particles implanted during the deposition of ta-C by the arc process. For this purpose, substrates (roughness Ra ~ 0.03 µm) were coated coated with ta-C (roughness ~ 0.07 µm) and then post-treated with a wire brush. During brushing, the normal force between brush and coating, the processing time as well as the brush (SS wire with thickness 0.2 mm and 0.5 mm) were varied.

In Figure 15c and 15d it is clear that the roughness is inversely proportional to both the machining time and the force applied during brushing. After only 5 s of machining time (speed: 7000 rpm, normal force 60 N), a significant reduction of the surface roughness to values of up to Ra ~ 0.025 µm can be seen. Here, brushes with thicker wires lead to lower roughness at shorter machining times. A similar behaviour is shown depending on the speed of the wire brush used. At a speed of 3000 rpm, for example, the roughness is Ra ~ 0.05 µm, while at 7000 rpm roughness of R ~ 0.025 µm can be achieved with otherwise identical parameters.

In summary, the evolution of roughness development for the coating process used is shown in Figure 16. It becomes clear that relatively smooth substrates are roughened by the pretreatment by metal ion sputtering. A smoothing of this roughness is partly achieved by the subsequent step of chromium deposition. However, the final coating step, vapor deposition with carbon, again leads to an increase in roughness. This is mainly due to carbon particles from the arc process (see Figure 16b).

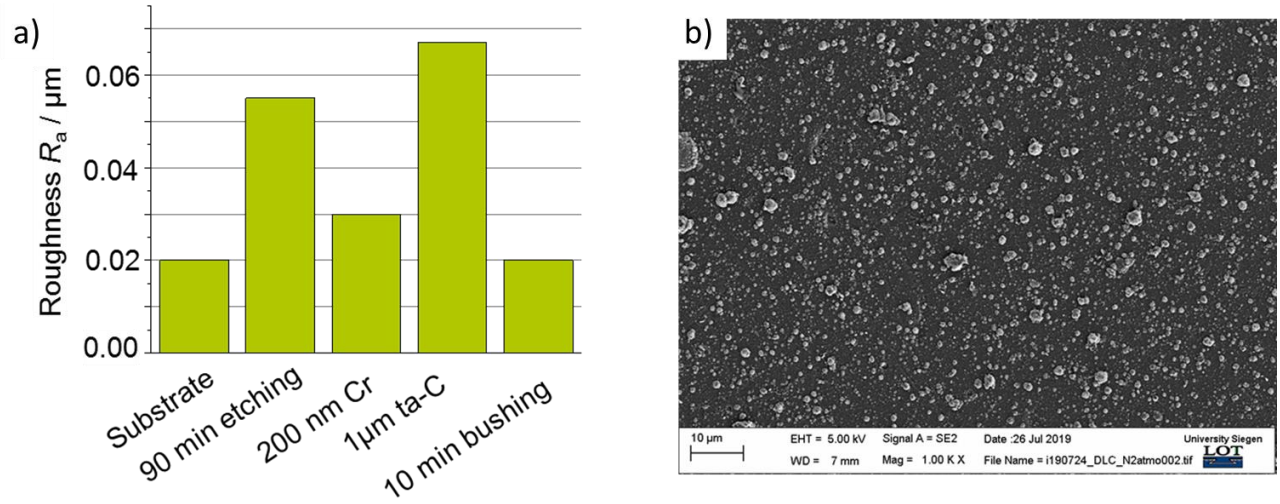

Fig. 16: a) Exemplary representation of the Ra values as a function of the processing steps performed during PVD coating using arc processes. b) SEM representation of a nitrogen-doped ta-C coating.

Based on these results, an attempt was made to pre-treat tools in such a way that scoring/roughness was introduced both parallel and orthogonal to the tool axis. The aim of these experiments was to change the topography in such a way that a surface texture on the component surface is measurable even after the deposition of the coating and the subsequent polishing of the samples. For this purpose, the samples were machined using 500 abrasive paper as well as by milling. The results of the milling as well as illustrations of reference samples are shown in Figure 17. Furthermore, it can be seen that the grinding of the samples did not allow sufficient roughness to be introduced into the tool surface.

The surface textures were almost completely removed by polishing with a wire brush (see e.g. the removed grooves in Figure 17c and 17d). Only deeper grooves (up to 10 µm deep trenches), which were made with a lathe, could still be measured after coating and brushing the samples. An expected advantage of texturing (mechanically or by laser structuring) the tools before coating is that the coating properties are not changed by a subsequent process, e.g. a laser process. Thus, it could be shown that laser structuring using DLIP and an ns-laser can have a positive influence on wear, but in some cases the coefficient of friction was also increased (see section 4 for additional information). One reason for this is that the laser process converts the ta-C layer locally into a-C or sp2-rich areas. This conversion can be avoided by structuring the tool before coating or by using an ultra-short pulsed laser source.

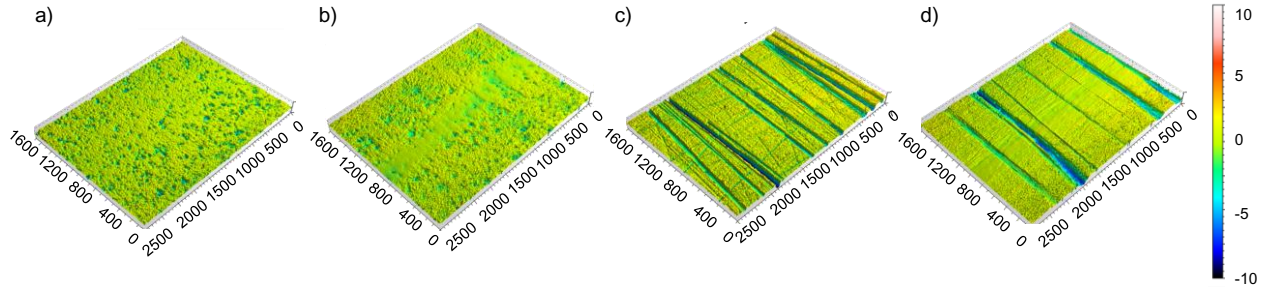

Fig. 17: Microscopic image of a) coated, b) coated and polished, c) textured and coated and d) textured, coated and polished tools for strip tensile tests.

As has been shown, however, the texturing must be carried out in such a way that it is not removed again by necessary polishing processes of the layer. Deviating from the project planning, the influence that coating of sheet metal for strip tensile bending tests can have was also evaluated. For this purpose 1 m long sheet metal strips were coated with 3.6 µm ta-C. This enables statements to be made about the behaviour of the coating in relation to both coated and uncoated tools. Furthermore it will be shown which influence the strip tensile bending test will have on the coated sheet metal strips.

3.2 Tribological and mechanical porperties of the deposited coatings

An essential parameter in the tribological evaluation of the properties of ta-C coatings is the coating hardness [14, 15, 16]. This has a direct influence on the friction coefficient of the coatings used. Various studies have shown that the hardness of the coating is proportional to the modulus of elasticity of the coatings [17]. However, experiments in the second phase of the project had shown that the E-moduli of layers from one batch can be very different and that these tools can only be used for comparable tribological investigations to a limited extent. The fluctuations here were between 350 - 420 GPa. It can be expected that the angle of incident during the coating process is influencing the thin film properties as it was also found in the literature [18]. An explanation of these fluctuations is related to subplantation model [19, 20]. According to this model, the ion energy or the subplantation depth of the ions is decisive for the layer morphology. Too low or too high penetration depths (ion energies) result e.g. in sp2-rich softer layers. Therefore, the influence of tool positioning within the vacuum chamber (Figure 18) was evaluated. The following influencing factors of the positioning of a coating in 1-fold rotation were determined from test experiments:

a) The tools were not aligned with the apex (see Figure 18) to the evaporators. The modulus of elasticity can change depending on the angle.

b) The tools can be arranged differently between the evaporators. This can also result in varying coating angles.

In the following, all tools were therefore positioned according to Figure 18b and aligned with the apex when the tool is directly in front of the evaporator.

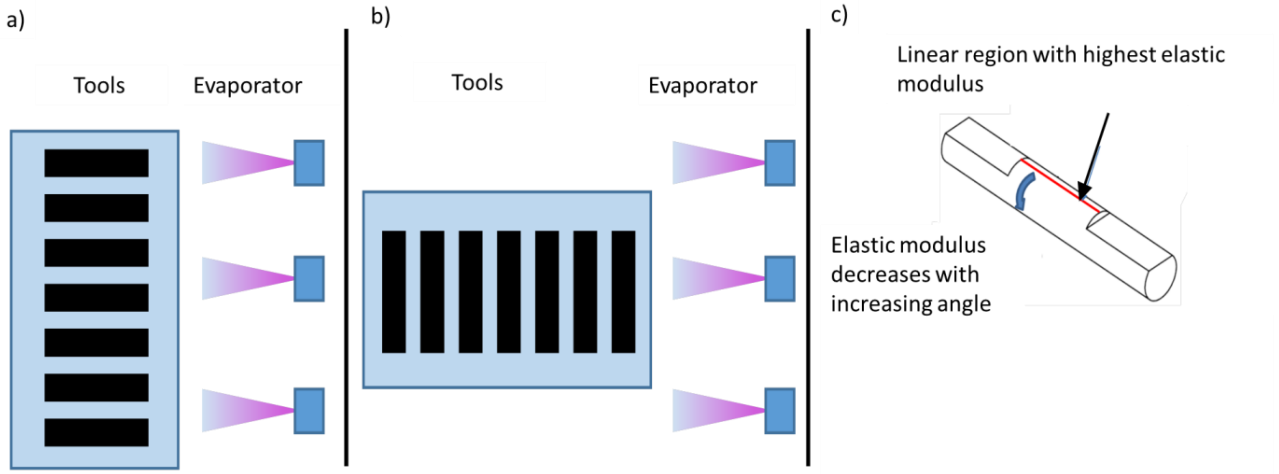

Fig. 18: a) and b) Schematic representation of possible sample positioning within the coating chamber used. c) Schematic representation of the coated tools.

As an alternative solution to reduce the variation in coating hardness of 3D components, it is advantageous to apply a BIAS voltage during the coating process. This voltage should change the angle of incidence of the carbon ions so that they strike more orthogonally to the sample surface. A further possibility for homogeneous coating of rotationally symmetric tools is the deposition in 3-fold rotation, which results in a homogeneous coating. However, the reduction of the effective coating hardness can be a disadvantage.

A further essential prerequisite for the functionality of the deposited layers is the layer adhesion, which has already been a major focus of investigation in the first project phase. At the beginning of the second project phase it was demonstrated that improvements in the tribological properties (in terms of higher hardness) of the ta-C coatings can be achieved due to lower pressures during coating (reduction of the coefficient of friction in

strip tensile bending tests from 0.18 to 0.13, see Table 1). Initial wear investigations using a ball-on-disc tribometer (100Cr6 ball vs. ta-C) have shown that the coating wear is inversely proportional to friction. Two samples with a hardness of 21 GPa and 24 GPa were compared. No wear was visible on the 21 GPa sample, while for the 24 GPa sample clear signs of wear were observed.

3.3 Modification of the coating properties

In further work, the fundamental question was raised whether the properties of ta-C layers can be further optimized. Two aspects in particular were examined:

a) The possibilities of reducing the layer stresses at the ta-C/steel interface by adjusting layer gradients, especially in point load scenarios;

b) What possibilities are there to influence the coefficient of friction by doping ta-C with fluorine.

Potential layer systems were simulated to set suitable layer gradients (see Figure 19). A maximum modulus of elasticity of the layer of 400 GPa and 500 GPa at a layer thickness of 5 µm was assumed as an example. In addition, the Young's modulus was reduced in 1 µm steps starting at the surface (OF) in the direction of the substrate (IF for interface) as well as in opposite steps of 50 GPa. The simulated indenter (diameter 100 µm) was pressed onto the surface with a force of 10 N.

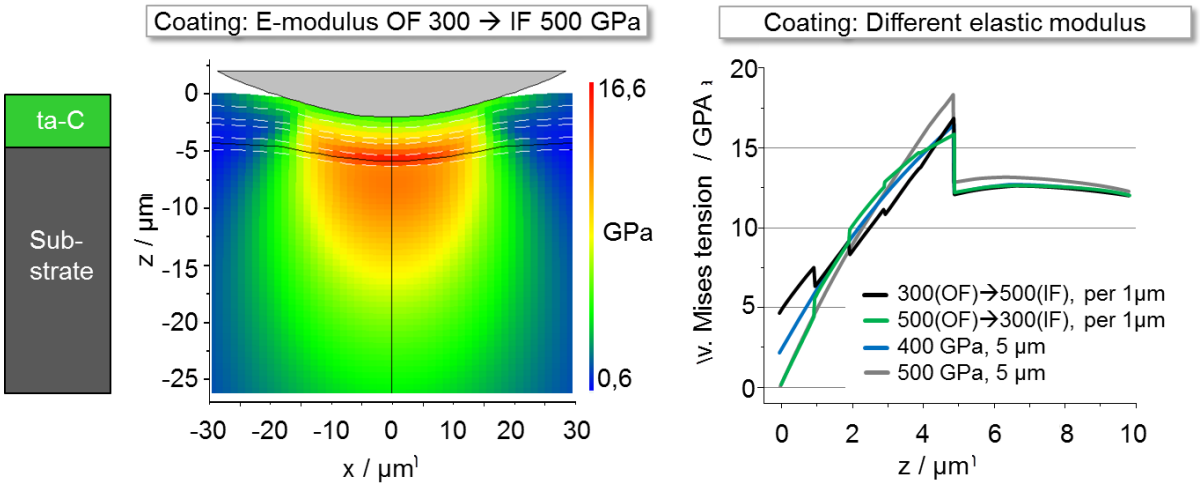

Fig. 19: Schematic representation of the simulated layer system consisting of ta-C layer and substrate as well as the van Mises stress in the layer system as cross-section as well as at the position x = 0 µm and along the z coordinate.

It was shown that in the selected loading scenario, the van Mises stress at the interface (IF) is highest in the layer with the highest modulus of elasticity. In contrast, the lowest stress at the interface is found when the E-modulus of the layer is highest at the surface and decreases towards the substrate. It should be noted that the maximum stress can also be a function of the selected stress scenario. Experiments have been carried out to achieve such coatings by varying the chamber pressure during PVD coating. It was shown that at higher pressures during the coating process softer layers with a lower modulus of elasticity can be deposited. To achieve the lower chamber pressures, nitrogen was introduced into the vacuum chamber. However, it was difficult to verify the results shown by simulation in experimental tests.

In further experiments, fluorine-doped ta-C coatings were produced. For this purpose, coating parameters were selected according to the standard parameters (see table 2). In addition, CF4 gas was let into the coating chamber (see figure 14c) during processing. It could be shown that fluorine-doped layers can be produced, here the Fluorine content in the coating is a function of the relative amount of the same element in the coating chamber as well as additional process gases (in this case argon). The basic idea of additional gases is to increase the ionization rate of fluorine. At the same time, it can be seen that with a higher proportion of gas during the coating process, the particle density in the layer increases.

Due to increased requirements with regard to occupational safety and the climate critical properties of fluorine-containing gases, the work on doped layers was subject to considerable delays. Corresponding layers

could therefore only be deposited towards the end of the project (see figur. 20). Further investigations are planned for the future.

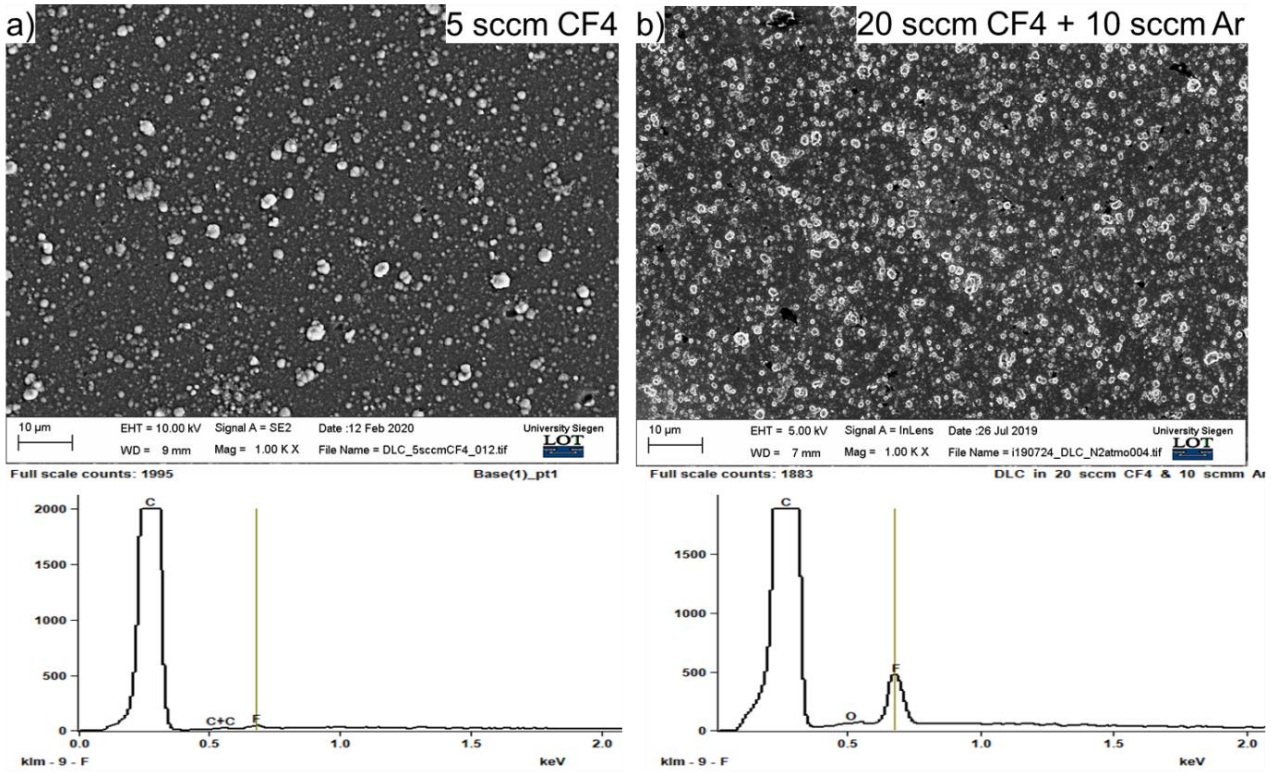

Fig. 20: SEM presentation a) a ta-C sample coated at 5 sccm CF4 and fluorine in the layer detected by EDX. b) a ta-C sample coated at 20 sccm CF4 + 10 sccm Ar and fluorine in the layer detected by EDX.

3.4 Modification of the ta-C interlayer

Interlayers between a tool and the ta-C coating itself are very important for the thin film adhesion, as it was shown in various publications [21, 22, 23]. With regard to these interface, it is important to consider both the substrate pretreatment and the use of adhesion-promoting layers. For adhesion promoting layers at ta-C it is important to use materials that have carbide forming properties. For this reason, chromium was used as an intermediate layer (see figure 21). Furthermore, chromium helps to improve the corrosion resistance of steels. For these reasons, only carbide forming and corrosion resistant layers or materials can be considered as chromium replacement layers. In contrast to carbon, the material price of chromium represents a significant cost factor in the coating of components. In contrast to the use of an adhesion-promoting layer, this work package follows the approach of modifying the component surface by nitriding and using this newly formed surface layer as an "adhesion promoter".

First tests on stainless steels have shown that surfaces nitrided in this way have both a certain corrosion protection and adhesion promoting properties [24, 25]. For this purpose, the samples were subjected to plasma nitriding at low temperatures using an arc enhanced glow discharge (AEGD) process immediately before carbon coating. It was shown that 3D components, especially at edges and corners, can have field elevations and thus an increased nitriding. For this reason, the samples investigated in the following were produced using a plasma-assisted CVD process (PACVD).

Prior to the actual PACVD nitriding process, the samples were sputtered in the CVD coating unit. The nitriding process took place at a working pressure of 2.4 mbar und Argon as working gas. Also, the reactive gases N_2 (80 %) and H_2 (20 %) were used, and the temperature of the process was set to 550°C. The process was performed for 16 hours.

After the nitriding process, the surface of the substrates were treated with fine ¼ µm diamond suspension and were wetted and polished on a polishing machine. The coating systems examined in the following are represented in Figure 21.

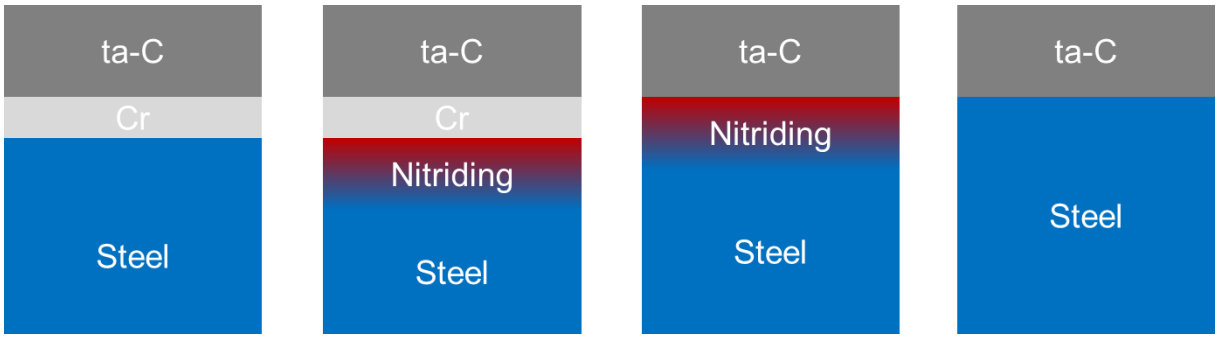

Fig. 21: Schematic representation of the layer systems examined in nitriding tests. ta-C with a chrome intermediate layer represents the standard layer system used. Variations to this are the avoidance of chromium as intermediate layer and/or the nitriding of the substrates.

The investigated coating systems were examined by means of Rockwell-C test as well as scratch test. The results of the scratch test are listed below:

Table 3: Adhesion properties of ta-C coatings with and without nitriding oft he steel substrates.

Property / Steel	**1.2379**	**1.2379**	**1.2379**	**1.2379**
Nitriding	No	No	Yes	Yes
Coating	ta-C + Cr	ta-C	ta-C	ta-C + Cr
Adhesive strength class	HF 1	HF 1	HF 1	HF 1
Roughness (µm)	0.05 +/- 0.03	0.05 +/- 0.03	0.06 +/- 0.03	0.06 +/- 0.03
Critical load Lc2 (N)	28 +/- 1	25 +/- 1	46 +/- 1	42 +/- 1

The critical load Lc2 was evaluated as a measurement for the scratch test. This indicates the critical load at which the first layer chipping occurs and thus an adhesive layer failure. It was found that nitriding the samples before coating leads to a significant improvement in the layer adhesion in a scratch test. This was applied to nitrided samples with and without a chromium intermediate layer.

3.5 Decoating of ta-C layers

Forming tools are relatively cost-intensive to manufacture and it is advantageous to regenerate or recondition them after appropriate wear. In addition, such repairs are necessary if a faulty coating has occurred, e.g. due to a process disturbance. Such repairs are usually very time and cost intensive. The use of appropriate friction- and wear-reducing tribological protective coatings can increase the service life of high-quality tools, but the cost of reconditioning these tools also increases. In order to make such tool repairs economical and time-saving, it was investigated whether there are effective possibilities to remove the applied coating systems. Due to the good layer adhesion and high hardness of diamond layers, the mechanical removal of material is very costly and can generally be excluded as a manufacturing process. Optical processes such as laser ablation are suitable in principle for removing of hard coatings [26], but they are either cost-intensive and slow, as multi-pulse processing with ultra-short pulsed lasers is required, or they damage the starting material due to excessive energy input. This can lead to melting of the component surface and further necessary process steps, such as mechanical post-processing of the surfaces, may be necessary. For these reasons, chemical surface processes are promising alternatives. However, it should be noted that carbon layers are in principle inert to many etching agents. There are works where mixtures of potassium dichromate, $K_2Cr_2O_7$ and sulfuric acid H_2SO_4, or sulfuric and nitric acids HNO_3 were used to remove or activate carbon, but these processes are very time consuming, of even several hours [27, 28].

A promising alternative approach is the possibility to remove the chromium adhesion promoter layer between the tool and the ta-C layer. In this context, two methods, the so-called "tampon method" as well as an approach using a potentiostat (three-electrode structure) were investigated. In summary, it was shown that the tampon

process has advantages, among other things, with regard to the process speed. Figure 22 shows the roughness of samples that were decoated at a voltage of 10 V and different media (caustic soda and sulphuric acid).

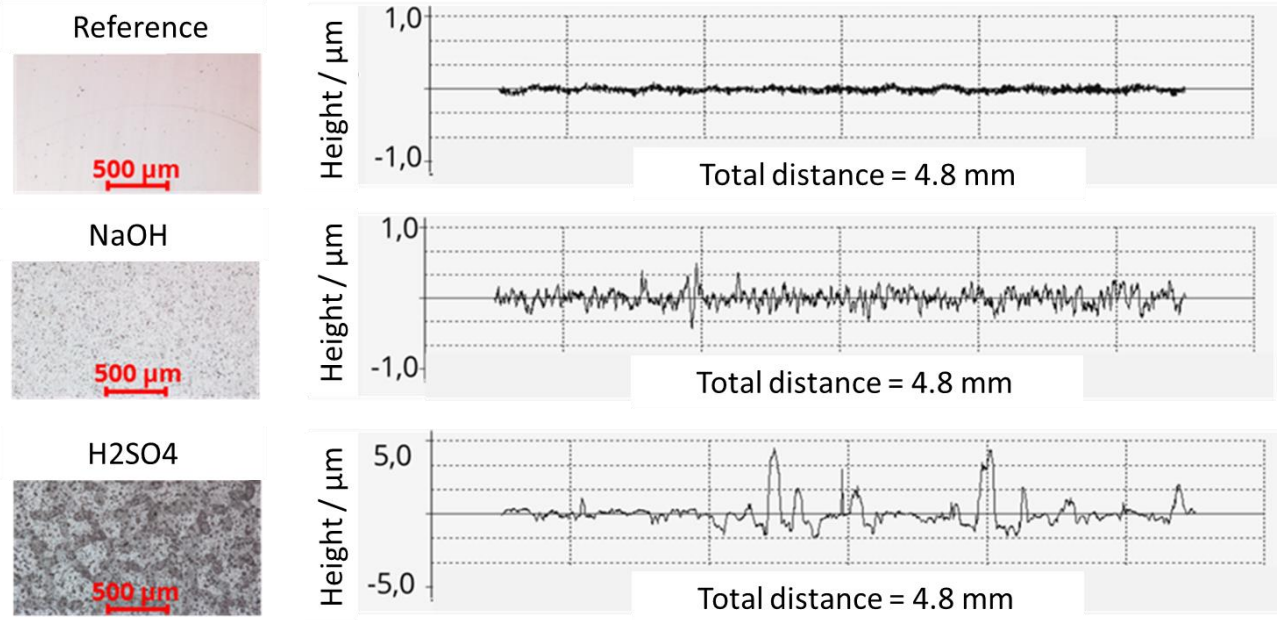

Fig. 22: Comparison of the decoated surfaces at 10 V with the different solutions, versus the substrate material (reference). On the left side microscopic images of corresponding surfaces. On the right side, images of the corresponding tactile roughness.

It was found that caustic soda, in particular is excellently suited for removing coatings while at the same time producing relatively low roughness. The multiple coating and decoating of the samples could also be successfully demonstrated. Critical is the disposal of the resulting caustic solution, which contains CrIV according to its coloration.

4 Micro-structuring with Direct Laser Interference Patterning

It is known that smaller effective contact areas can provide surfaces with a lower frictional force as demonstrated by different authors [29 - 32]. Thus, in this project, both the tool as well as the metallic blanks were micro-structured with the aim of minimizing friction and wear.

In particular, Direct Laser Interference Structuring (DLIP) was used as an innovative laser process to produce sub-µm and µm structures directly on different materials [33, 34] by fabricating periodic surface structures which result from transferring the shape of interference patterns directly to the material' surface.

The principle of the DLIP is shown in Figure 23. As it can be seen, the primary beam is split by diffractive optical element (DOE) into at least two coherent partial beams. These sub-beams are brought to interference at a certain angle (θ) on the surface. Due to the interaction between the substrate material and the laser radiation, a periodic pattern in the micro or submicrometer range is created. The type of structure depends on the number of laser beams used Thus, line or dot-like patterns can be produced with two or three laser beams, respectively. Grid-like structures are also possible by irradiating the surface of the material two times, before rotating the sample by a certain angle (e.g. 90°) between the irradiation steps [35, 36, 37].

The size of the structure or the periodic distance (Λ, distance between two maxima or minima) is determined by angle (θ) between the laser sub-beams and can be generally varied to obtain spatial periods between 150 nm and approximately 40 µm [38 - 43].

In this project, the used DLIP optics allows changing the distance between the beam splitting diffractive optical element (DOE) and the prism (Figure 23b). Consequently, the angle θ and the spatial period can be changed automatically. The positioning of the substrate is performed using XYZ-precision stages as shown in Figure 23a.

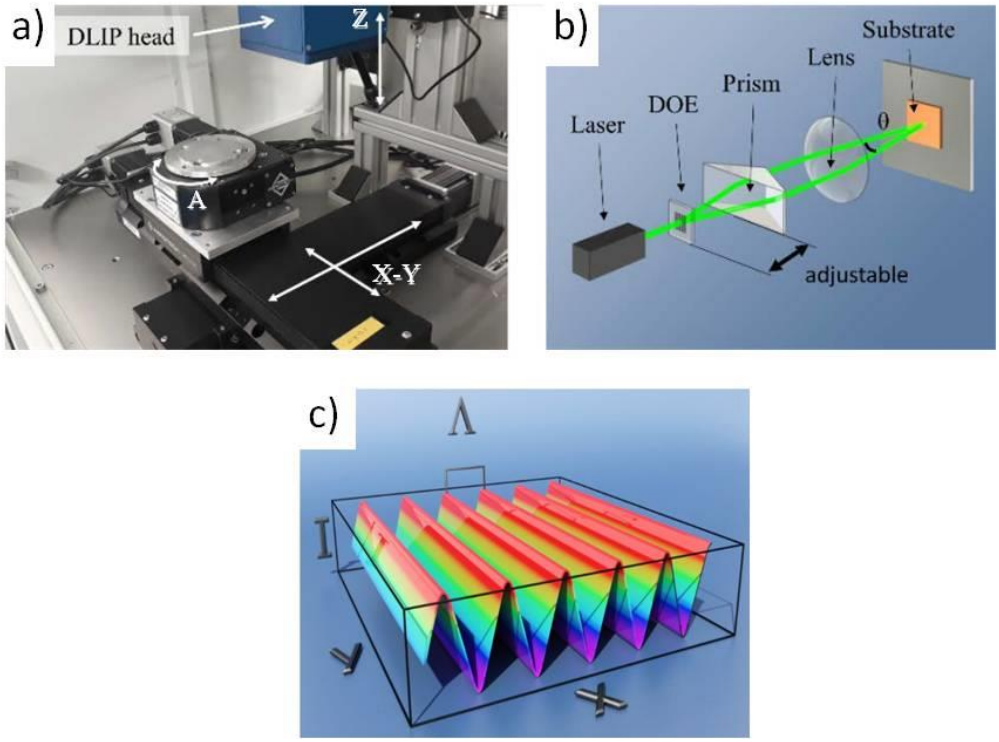

Fig. 23: DLIP-setup with a DLIP optical head, XYZ linear stages and a rotation axis, (b) Principle of the optical configuration for two-beam DLIP using a DOE, a prim and a lens. (c) Resulting laser intensity distribution within the interference volume.

The DLIP method has been successfully used for structuring semiconductors, metals, polymers and ceramics [44 - 47]. Furthermore, the structuring takes place within one process step. Additional processes such as photoresist development or the transfer of structures by chemical or physical etching processes are not necessary. Thus, the DLIP process offers the possibility to create the desired structures over a large area and at a throughput speed of several cm²/s.

The area that can be structured with a laser pulse depends on the size of the laser spot (up to a few cm²), whereby this is determined by the choice of suitable optical elements (e.g. lenses). In addition, the DLIP offers the possibility to process complex component geometries (e.g. cylinders) easily and quickly, since the interference structures are created in the volume of the overlapping laser beams. Some examples of structures on ta-C coated steels are shown exemplary in Figure 24. Note that the spatial period in Figure 24a was 180 nm. In Figure 24b, characteristic rainbow-color effects (TU Dresden logo) are visible due to the high-quality of the produced periodic structures.

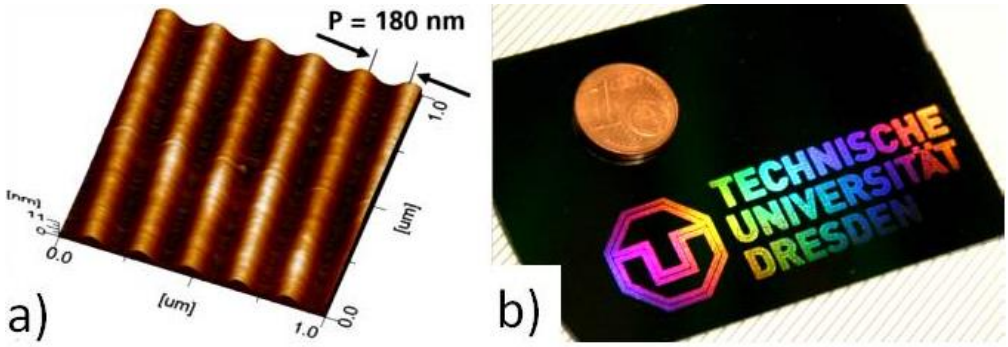

Fig. 24: a) Direct Laser Interference Patterning on ta-C with period of 180 nm and one laser pulse. b) TU Dresden logo produced on ta-C coating with DLIP.

4.1 Optimization of friction-minimized functionalities on ta-C coated tools using DLIP

The realization of a load-compatible, lubricant-free deep drawing process requires a significant improvement of the tribological properties, especially at the drawing edge radius. Here the introduction of a microstructure can make a significant contribution. For this purpose, selected ta-C layer systems (with hardness values up to ~ 650 GPa) were processed direct laser interference patterning.

4.1.1 Influence of DLIP structuring on morphology and friction behavior of ta-C

Based on the wavelength dependent rehybridization thresholds of the ta-C layer, the material behaviour due to DLIP was investigated [48]. Figure 25a shows the structured area of a ta-C surface where interference patterns with a spatial period Λ of 2.3 µm was used. The line-like geometry of the structure resulted from the interference pattern produced using a two-beam DLIP optical head. In this case, the laser wavelength was 263 nm and a nanosecond pulse length (~2 ns) was used.

Due to the Gaussian intensity distribution of the output laser beam, a gradually changing intensity of interference patterning occurs on the ta-C surface. For example, the "area 1" in Figure 25a (see further details in Figure 25b) shows that for small laser fluences the rehybridization threshold of ta-C is exceeded at the positions of the interference maxima. As a result of the energy input into the material, the transformation of sp3- into sp^2-hybridized carbon occurs. This leads to a local reduction of density combined with a localized bulging of the ta-C layer. A further increase of the laser fluence at the positions of the interference maxima leads to an exceeding of the ta-C ablation threshold and thus, as shown in "area 2" of Figure 25a (see also Figure 25c), to a gradually increasing ablation of the strongly sp^2-containing areas. At the same time, there is a material bulge at the positions of the interference minima, which can be explained essentially also by a sp^3-sp^2 transformation, which is again associated with a local density increase, but in this case due to thermal diffusion. This effect is particularly pronounced for small spatial periods (Λ < 5µm).

At the position indicated as "area 3" in Figure 25a and 25d, the material regions which are adjacent interference maxima converge (these zones are rich in sp^2-hybridized carbon) and a higher features are formed. The structuring mechanism is also schematically shown in Figure 25b, where the function I(x) indicates the spatially resolved laser intensity of the interference pattern.

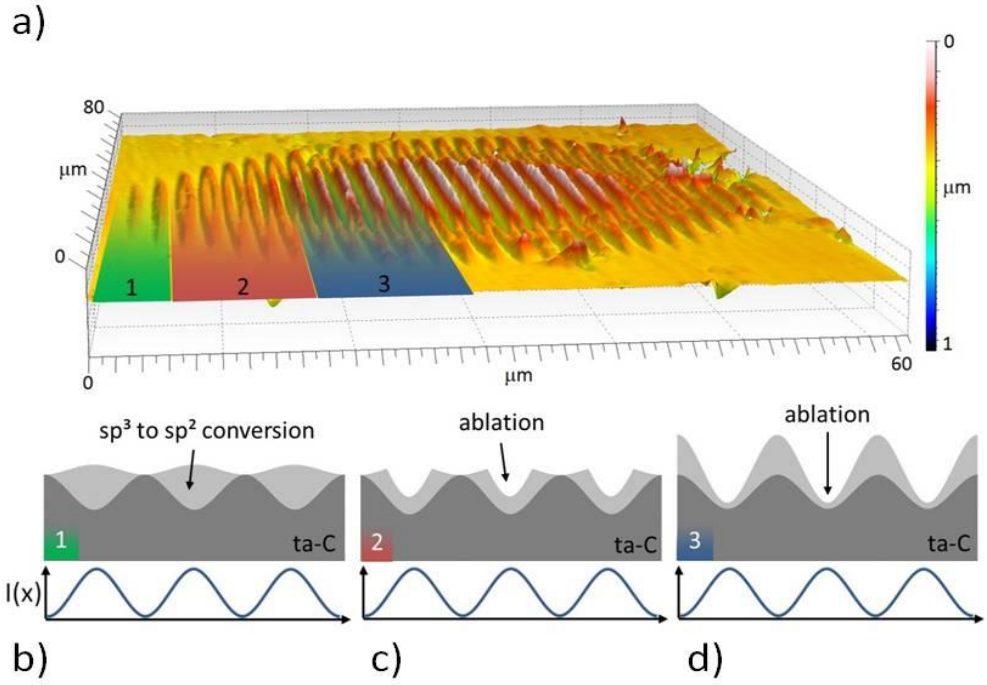

Fig. 25: (a) Example of DLIP patterned ta-C surface. Schematically presentation of (b) locally transformed ta-C surface due to laser irradiation, (c) initial ablation of sp^2-rich areas and (d) complete ablation of sp^2-rich areas. The function I(x) represents the spatial laser intensity.

The structuring process performed using nanosecond laser pulses was simulated using finite element methods (FEM). The simulations allow for example to evaluate the dependence between different interference periods and the resulting thin film heating during the material processing. These simulations are based on the heat diffusion equation as it was published elsewhere [15].

In Figure 26, thermal simulations, based on the experimental parameters are shown. As a guide for the eyes, the 1000 K adiabatic curve is indicated as a black line. The selected temperature distributions were taken when the highest temperatures at the ta-C/air interface (at the interference maximum) is reached. Here a maximum temperature of 4620 K is reached 8 ns after the maximum pulse intensity (Gaussian temporal pulse shape). These temperatures are above the sublimation temperature of ta-C (around 3915 K) and thus thin film ablation occurs. A comparison of the peak temperature at the ta-C/air-interface and the temperature at the interference minimum positions reveal major differences. With decreasing interference period, the temperature at the interference minimum position increases. For instance, at a DLIP period of Λ = 2 µm a maximum temperature of 1300 K is observed (see Figure 25a). The reader should note that a peak temperature of 1400 K is reached 20 ns after the maximum pulse intensity (data not shown). Since the graphitization temperature of ta-C is about ~1000 K we expect a structural modification of the thin film surface is modified.

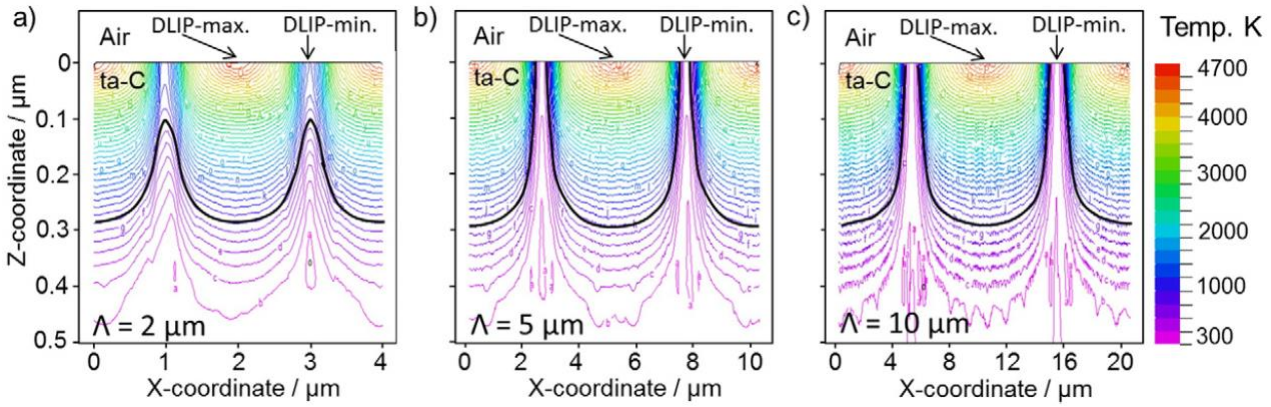

Fig. 26: Thermal simulations for structuring with periods of Λ = 2, 5 and 10 µm. The black lines indicate the temperature for sp^3-sp^2-rehybridization (at 1000 K).

From the simulations, it becomes apparent that the heat-affected zone (or amount of hybridized material) is more pronounced for smaller interference periods (Λ = 2 µm, see Figure 27a), whereby the rehybridization threshold of ta-C is exceeded in extended surface areas (interference maxima and minima). In contrast, larger interference periods such as 5 µm or 10 µm (see Figures 27b and 27c, respectively) lead only to a rehybridization at the positions of the interference maxima and not at the interference minima. These differences in the rehybridized ta-C material can have a significant influence on the friction behavior and must be considered.

Different performed investigations, have shown that the sp^2-rich areas presenting different morphologies (line, hole or cross structures) produced by Direct Laser Interference Patterning can influence the friction properties of tribologically interacting surfaces depending on the applied load and speed conditions [15, 39, 49].

For example, cross-like structures produced by the two-step procedure explained above showed a significant improve on the friction coefficient. The structuring process was carried out on a ta-C layer with a thickness of 2.5 µm using a ns-pulsed UV laser system with a wavelength of 355 nm. The non patterned ta-C layer as well as the manufactured cross structures are shown in Figure 27a-d, and have structure periods Λ of 2.0 µm, 5.0 µm and 10.0 µm. The influence of the structure period on the friction behaviour of ta-C was investigated using ball-and-disc friction tests under non-lubricated conditions, and the obtained results are shown in Figure 27e. It can be seen that the friction behavior of ta-C can be both increased and decreased depending on the structural period. In general, larger structural periods were found to be more favorable compared to the unstructured ta-C reference layer. The reason for this behavior can be explained by the performed thermal simulations, since a lower amount of rehybridized material is produced (note that the hardness of the ta-C coating is proportional to the sp^3-carbon content).

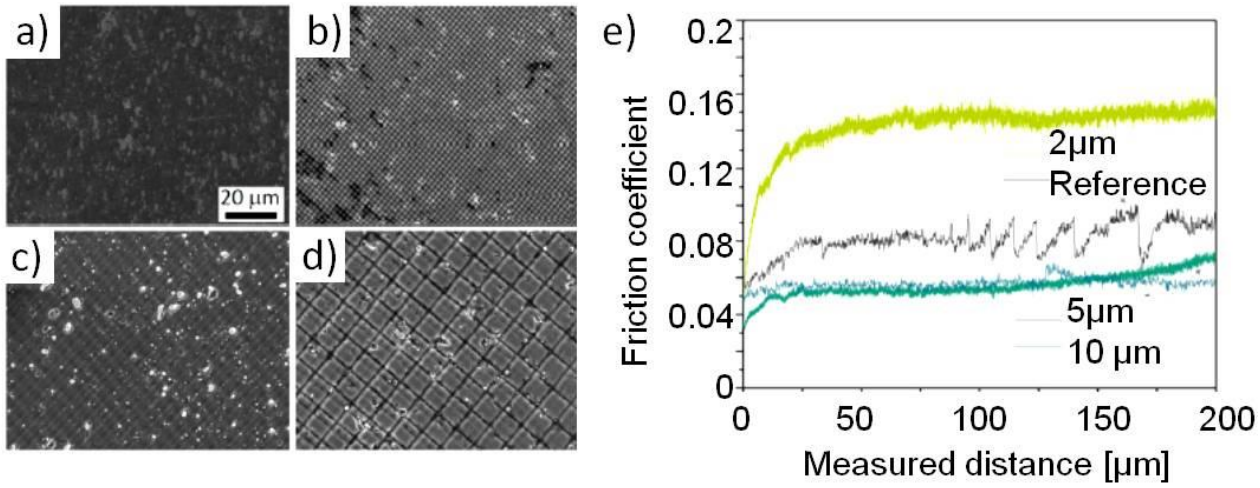

Fig. 27: Scanning Electron Microscope images of (a) unstructured ta-C surface and cross-like structured ta-C surfaces with spatial periods of (b) 2 µm, (c) 5 µm and (d) 10 µm. The influence of the surface structuring on the friction coefficient is shown in (e).

4.1.2 DLIP structuring of ta-C coatings using ultra-short laser pulses

As shown in the previous section, DLIP systems utilizing pulsed laser system can significantly influence both the morphology and topography of ta-C coated tools. For further minimize thermal effects as well as the surface contact are (by producing even more precise topographies), ta-C coated substrates were also micro-structured using ultra-short pulsed laser system (pulse duration ~ 10 ps). This was performed to investigate the essential, fundamental differences in material-beam interaction, especially with regard to thermal input.

The basic investigations on micro-structuring using DLIP with picosecond pulses was carried out on a selected ta-C layer with a modulus of elasticity of 610 ± 8 GPa and a thickness of 1.8 ± 0.1 µm. The DLIP system consisted on a 70 ps pulsed laser source (with a wavelength of 1064 nm) and different laser fluences (from 0.74 J/cm² to 2.03 J/cm³) were used. Also, different pulse-to-pulse overlaps (0 % - 90 %) were utilized and the spatial period was set to a spatial period of 5 µm. The microstructures generated on the ta-C coated steel were analyzed with respect to their surface topology (by confocal microscopy and SEM) and composition (by Raman spectroscopy). These results were compared with the topographies corresponding to ns-DLIP produced microstructures.

The fundamental topographical differences as a result of the different pulse lengths are reflected in the emerging surface topography of the generated DLIP structures (see Figure 28). When ta-C is processed with a ns-laser source, sinusoidal structures are increasingly formed at a fluence of approx. 0.6 J/cm². The resulting structure heights increase with increasing laser fluence up to ~300 nm (the cross-section of this topography is shown in Figure 28b). This is mainly due to the sp^3-sp^2 rehybridization during laser irradiation as has been explained before. Starting at a laser fluence of approximately 1.3 J/cm², the increasing laser intensity at the interference maxima leads to a local ablation of the sp^2-richer structure maxima. Differently, the structuring process with a ps-laser source, shows only a limited expression of the sp^3-sp^2 rehybridized areas even at higher fluences of up to 2 J/cm². The achieved structure heights are up to 100 nm (see cross-section of a ta-C coated surface treated with 70 ps IR radiation in Figure 28c), which can be explained with the shorter thermal diffusion lengths.

A complementary analysis of the generated DLIP surface structures with the ps-laser source by scanning electron microscopy (SEM) shows the additional pronouncing of wave-shaped trench structures with a structural period of about 800 nm. The observed substructures were identified as so-called laser induced periodic surface structures (LIPSS) (see Figure 29a). In general, the structural period and orientation of the LIPSS is significantly influenced by the laser properties used, such as the wavelength and polarization [50,51]. Due to the geometry and size of the here reported structures, they can be recognized as low spatial frequency LIPSS (LSFL), which typical spatial periods which are similar to the used laser wavelength (1064 nm) [52]. The SEM investigations show for all investigated fluences the presence of LSFL at the areas corresponding to the interference maxima (see Figure 29a and 29b), for low and high laser fluences. The presence of the LIPSS surface structures in combination with the already well controllable DLIP structures opens new possibilities for surface

functionalization. It is expected that a combination of DLIP and LIPSS structures (so-called hierarchical structures) can have a significant influence on resulting surface functions, such as wettability, optical properties or antibacterial effects, following nature's example.

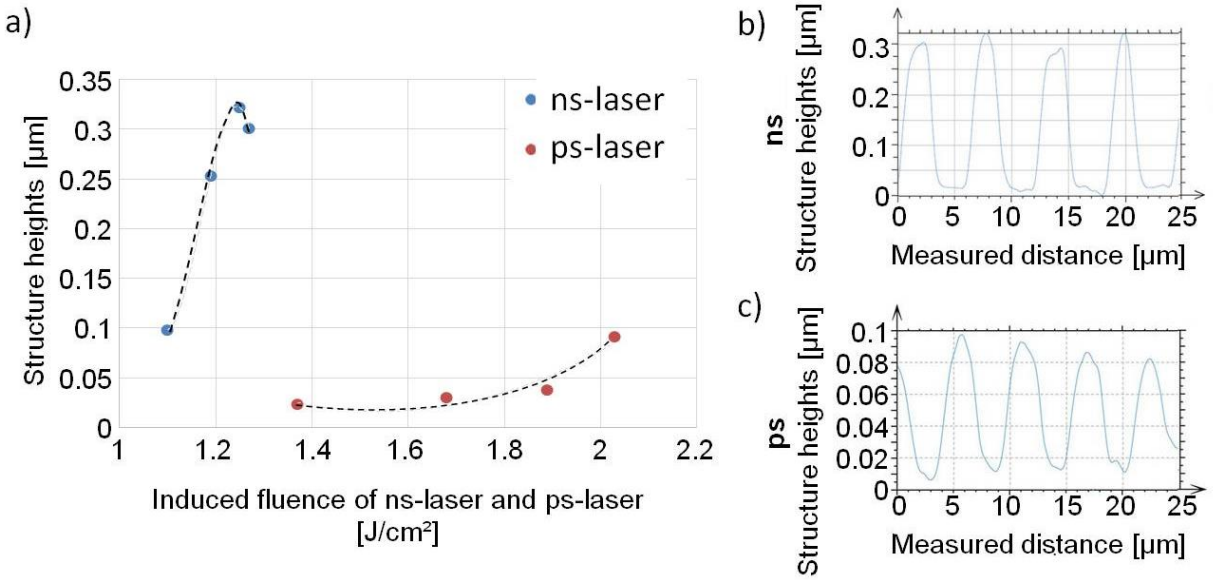

Fig. 28: (a) Comparison of structure heights for ns- pulsed laser and ps-pulsed laser structuring on ta-C. The diagrams in (b) and (c) show the peak formation for the ns and ps structuring cases.

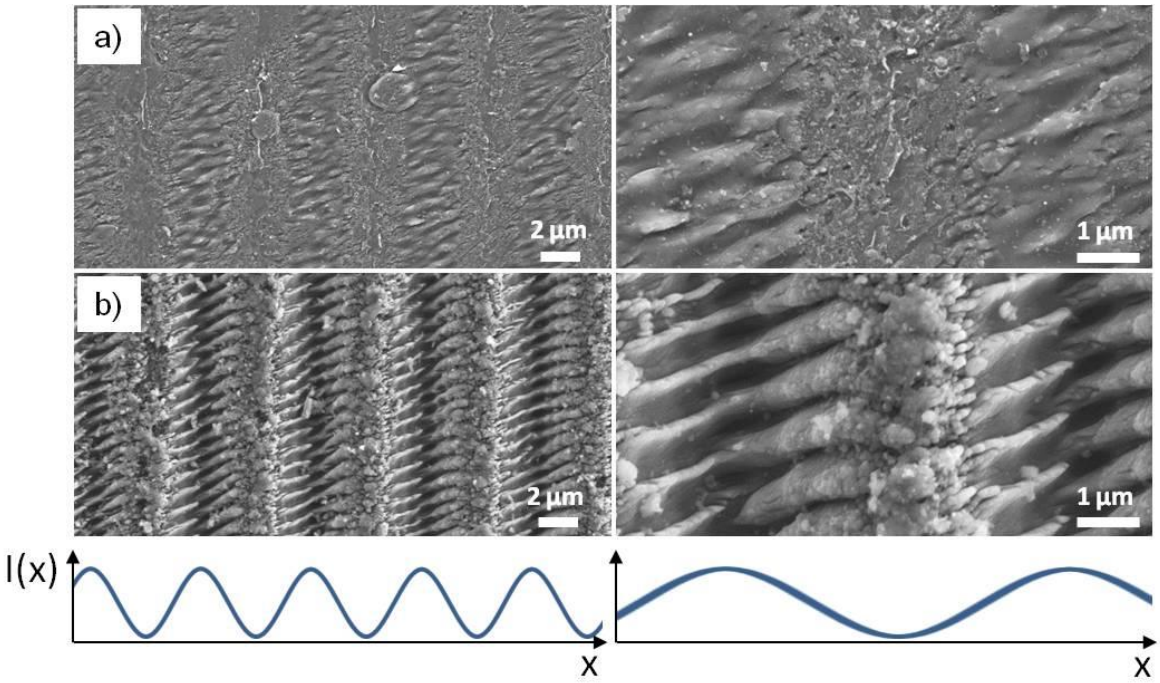

Fig. 29: SEM images of DLIP produced structures using 70 ps laser pulses (at 1064 nm wavelength). Laser fluence: (a) 1.52 J/cm²; (b) 2.03 J/cm². Low spatial frequency LIPSS (LSFL) were found at the interference maxima positions.

Raman analysis of both ta-C coated samples treated with both ns and ps pulses were also performed (see Figure 30). On the one hand, the analyses show that at the used laser fluences, there are no chemical changes at the intensity minima positions. Differently, for both ps and ns DLIP processes, an increase in the structural order along the direction outlined in Figure 30 within the ta-C material was observed [53]. From the intensity ratio I(D)/I(G) in combination with the width and position of the G-peak, ns-DLIP processing results in a stronger

order character and, as a consequence an increased content of graphite-like material-bound regions [54]. Conversely, in the case of ps-DLIP processing, a near-surface rearrangement of the sp²-rich areas can be assumed due to the lower structure height in combination with the attenuated I(D)/I(G) peak ratio.

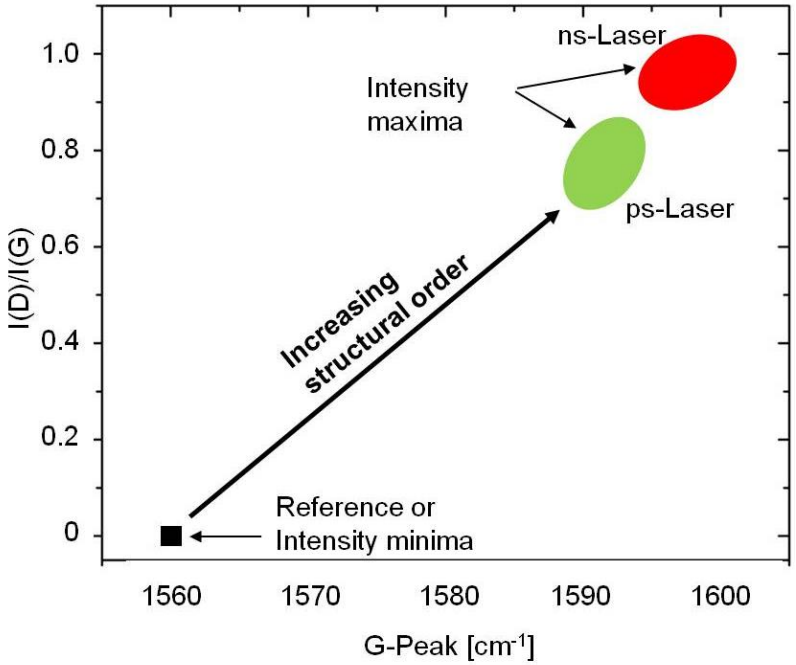

Fig. 30: Raman measurements for ns-laser and ps-laser structured surfaces on line-like structures. At the intersity minimas no structural change occurs, whereas an increase in the structural order is shown for the intensity maxima.

For the evaluation of ultra-short pulsed DLIP structuring on ta-C coatings, micro structures with spatial periods of 2.0, 5.0 and 7.0 µm were introduced on ta-C coated steel surfaces with line- and cross-like geometries. Optical evaluation of the DLIP-pattern was performed by Confocal Microscopy measurements and Scanning Electron Microscopy images. Ten samples were coated by a tetrahedral amorphous carbon layer of 2 µm thickness and a sp³-content between 60-70%, with a hardness of ~ 45 GPa and a Young's modulus of 360-450 GPa. These surfaces were brushed to a surface roughness of Sz = 1.77 µm. Two specimens were left uncoated for reference measurement. All samples were ultrasonically cleaned with ethanol for five minutes individually to remove contaminations from the surface. Micro-structuring of ta-C surfaces was performed with a 10 ps pulsed laser with a 1064 nm wavelength and 1 kHz repetition rate, 99% overlap in x and 80% overlap in y-direction. The laser fluence F_P per pulse was varied between 0.789 J/cm² and 0.309 J/cm², where the lower fluence was used in the second fabrication step for the cross-like structuring for not deteriorating the previous line-like pattern [55].

The resulting line-like and cross-like structures of the DLIP micro-structuring with the periods of 2 µm, 5 µm and 7 µm on ta-C surfaces can be seen in the SEM images of Figure 31 and the structure heights before the tribological testing in Table 3.

The influence of the ta-C coating and subsequent DLIP-structuring on the friction and wear behavior was tested, three times for each combination, using a ball-on-disk tribometer (Wazau, SVT3). A 100Cr6 ball with a diameter of 10 mm, cleaned with isopropanol, was pressed onto the sample surface as test counterpart with a force of F_N = 2N and slided with a deflection of 1 mm. The used frequency was 10 Hz and 36,000 cycles were measured, resulting in a test duration of 60 min. The record of the friction force F_F, ambient temperature and humidity was made at a frequency of 4 Hz. For the line-like patterns, the samples were positioned differently, to obtain tribological measurements depending on the orientation (parallel and orthogonal) of the produced line-like structures with respect of the ball movement direction. After the measurements, the surfaces were characterized by confocal microscopy and scanning electron microscopy, three times on different posi-

tions, without cleaning the surfaces after the tribological tests, and thus analyzing the presence of wear particles. The presented COF values are the average value of three measurements, taken after 60 minutes of measuring.

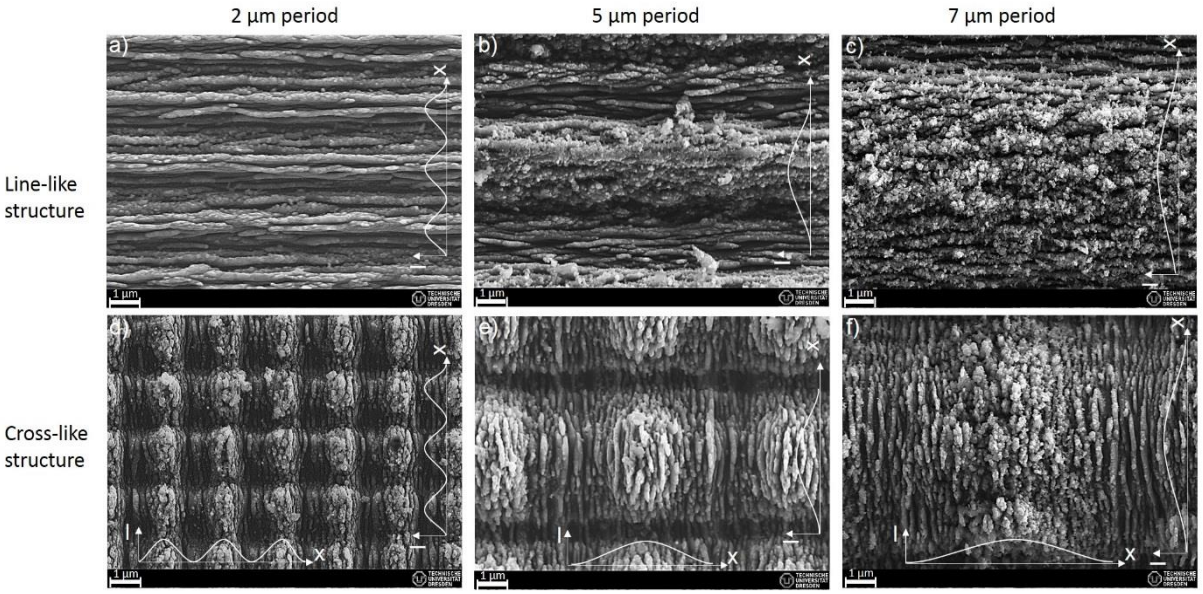

Fig. 31: SEM images of the DLIP structured ta-C surfaces with spatial periods of 2 µm, 5 µm and 7 µm aligned line-like (a-c) and cross-like (d-f). Laser Induced Periodic Surface Structures (LIPSS) are found superimposed on the DLIP structures and small graphs guide the eye to areas of structure maxima [55].

The lubricated steel samples show the lowest COF with 0.10, while the highest COF was measured for the unlubricated steel surface with 0.60 (see Table 3). Furthermore, the COF of the unstructured ta-C (0.18) is higher than any of the structured ta-C surface (0.11-0.17). The smallest COF on structured ta-C was found for line-like structures with 5.0 µm period, aligned parallel to the sliding direction. By comparing the depth and the volume of the wear tracks, as well as the remaining structure heights inside the wear tracks, an increase can be seen from small DLIP period of 2.0 µm towards the larger periods of 5.0 µm and 7.0 µm. Whereas the COF was higher for sliding orthogonal on the line-like structures, the depths of the wear track are slightly smaller and the remaining peaks in the wear tracks are slightly higher, compared to the values for sliding parallel on line structures or sliding on cross-like structures. It can be therefore concluded, a reduction of COF has the drawback of wear increase, which is in good agreement with the literature [49].

Table 3: Structure heights, COF and wear for the differently structured ta-C and references surfaces [55].

Sample	Original peak height ± SD [μm]	COF ±SD	Depth of wear track ± SD [μm]	Volume of wear track (x10³) ± SD (x10³) [μm^3]	Peak height in wear track ± SD [μm]
ta-C 2 µm ortho.	0.435 ± 0.051	0.17 ± 0.01	0.362 ± 0.033	54.9 ± 10.2	0.027 ± 0.010
ta-C 2 µm para.	0.456 ± 0.003	0.15 ± 0.01	0.466 ± 0.056	73.3 ± 8.2	0.019 ± 0.003
ta-C 2 µm cross	0.339 ± 0.063	0.17 ± 0.02	0.528 ± 0.071	112.0 ± 10.3	0.019 ± 0.002
ta-C 5 µm ortho.	1.315 ± 0.178	0.16 ± 0.03	0.890 ± 0.120	196.0 ± 33.4	0.485 ± 0.057
ta-C 5 µm para.	1.333 ± 0.131	0.11 ± 0.01	1.059 ± 0.079	223.0 ± 39.0	0.325 ± 0.092
ta-C 5 µm cross	1.147 ± 0.079	0.15 ± 0.02	1.095 ± 0.044	264.0 ± 49.7	0.213 ± 0.072
ta-C 7 µm ortho.	1.377 ± 0.023	0.16 ± 0.02	0.945 ± 0.047	208.0 ± 27.3	0.586 ± 0.033
ta-C 7 µm para.	1.380 ± 0.076	0.12 ± 0.01	0.968 ± 0.096	215.0 ± 29.0	0.489 ± 0.059
ta-C 7 µm cross	1.360 ± 0.037	0.15 ± 0.03	0.977 ± 0.117	198.0 ± 26.0	0.221 ± 0.008
ta-C unstruc.	-	0.18 ± 0.02	0.112 ± 0.028	12.3 ± 3.0	-
Lubr. steel	-	0.10 ± 0.03	0.153 ± 0.030	16.8 ± 5.4	-
Unlubr. steel	-	0.60 ± 0.08	9.919 ± 1.054	7130.0 ± 1150.0	-

SEM images of the structured ta-C surfaces after the tribological measurements can be seen in Figure 32a-c for 2.0 µm spatial period, Figure 32d-f for 5.0 µm period and Figure 32 g-i for 7.0 µm period. For the spatial periods of 5 µm and 7 µm, the line-like and cross-like DLIP structures show widened and flattened peaks but intact surface structuring in the valley positions. It can be seen further, that in the case of orthogonal sliding

(Figure 32d and g), the remaining plateaus are significantly wider than for parallel sliding (Figure 32e and h), which results in less space for wear trap and an increase in the tribological contact area, which agrees with the observed increase of the COF. For cross-like patterns and Λ = 5.0 µm period (see Figure 32f), the valleys are partly filled with wear debris, modelling a line-like structure similar to the parallel-slided line-like structure (Figure 32e).

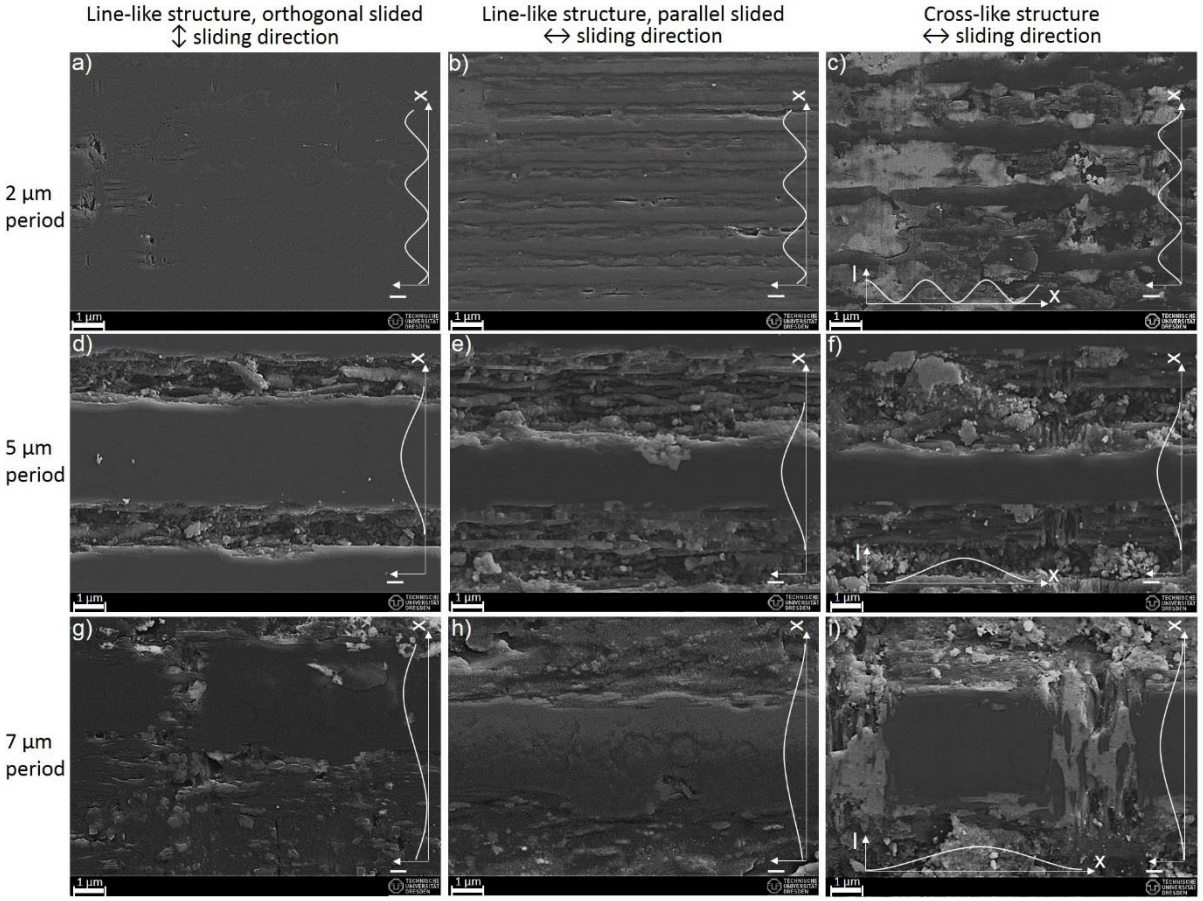

Fig. 32: SEM images after tribological measurements for line-like and cross-like pattern with Λ = 2 µm (a-c), Λ = 5 µm (d-f) and Λ = 7 µm (g-i) with respect to the sliding direction. Small intensity diagrams show the position of structure maxima [55].

4.1.3 Three-dimensional laser structuring of draw ring radii

During the deep drawing process, significant friction forces can be observed in the region of the drawing ring radius due to the wrapping of the work piece (see Figure 33a). Consequently, the drawing ring radius offers a huge potential for minimization of friction forces especially under lubricant-free conditions. Typically, draw-bend tests are employed to study the tribological behavior at the drawing ring radius [56].

In order to determine the influence of the ta-C coating as well as the structuring process on the friction behaviour, the active surface was completely and uniformly coated with ta-C layer of thickness 4 µm and then structured using the two-beam DLIP system. In this case, the spatial period Λ was set to 10.0 µm. Figure 33b shows a confocal microscopic image of the structured active surface. The topography of the treated area is also shown in the SEM image displayed in Figure 33c. In particular, from Figure 33b it can be clearly seen that despite the non-planar geometry of the tool surface, the DLIP structures are well defined all over the tool surface. However, local deviations of the structure period were observed. These deviations result from the curved geometry of the processed sample [57].

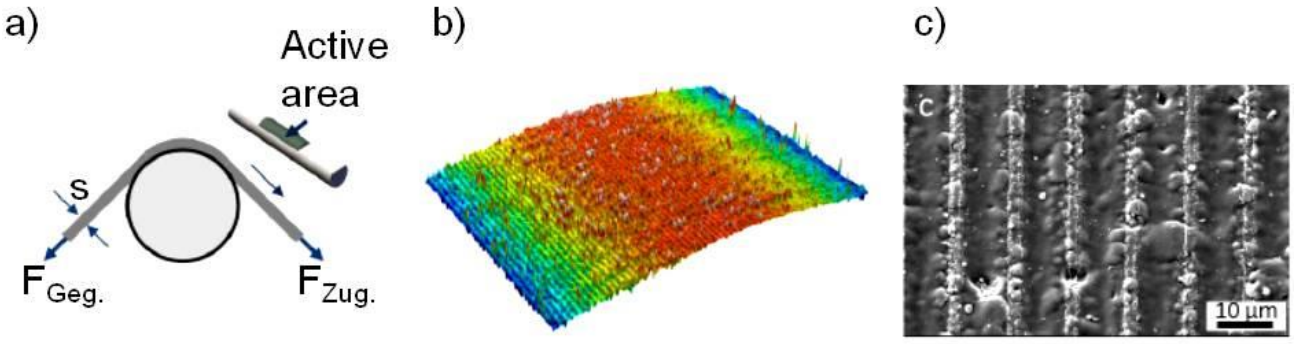

Fig. 33: Laser structuring of bend surfaces. (a) Representation of the drawing ring radius during the wrapping of the work piece (draw bend tests); (b) confocal microscope and (c) SEM images of DLIP treated curve surface of a ta-C coated tool.

Consequently, additional investigations focused on the influence of the tool geometry on the structure periodic of the patterns fabricated using DLIP were performed. Here, it was of fundamental interest to investigate how strongly the non-planar surface geometry influences both the local structure period and the structured area per laser pulse. While the former directly influences the structure geometry, the latter is highly important to determine how fast a forming tool can be processed. Note that the area of interfering laser beams is typically smaller (from hundreds of µm² to some cm²) compared to the total treated area. Consequently, the sample surface has to be moved relative to the interference setup to achieve a homogeneously textured surface.

For the structuring of curved surfaces, an experimental DLIP setup was developed, which is shown in Figure 34a.

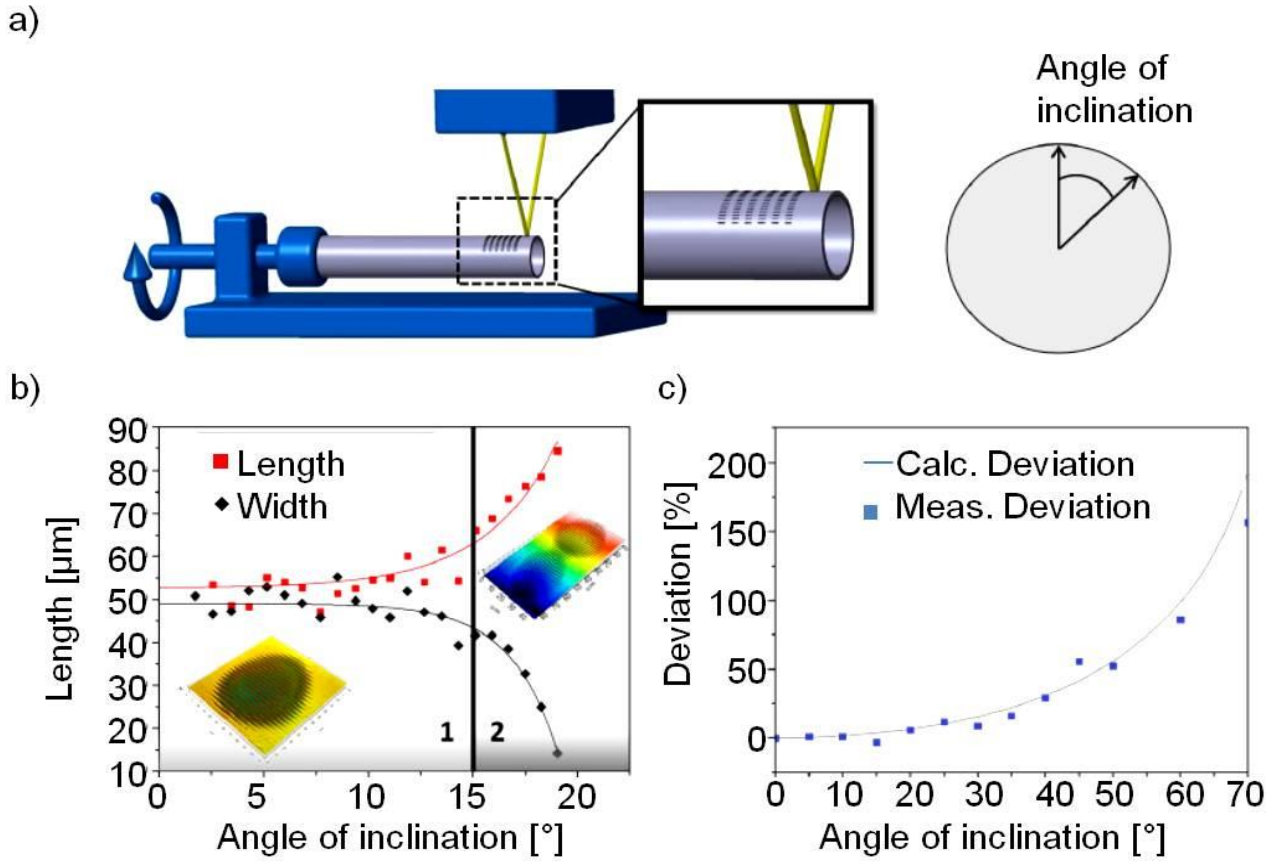

Fig. 34: (a) Experimental DLIP setup for the structuring of non-planar surfaces. (b) Observed deviations of the structured area in terms of length and width per DLIP laser pulse. The region 1 ($\gamma < 12.5°$) depicts an acceptable interference area with a homogeneous surface pattern, while in region 2 ($\gamma > 12.5°$), the interfering laser beams do not properly overlap. (c) deviation from the spatial period ($\Lambda = 2.3$ µm at $\gamma = 0°$) as a function of the surface tilt angle at constant working distance.

In order to determine the deviations from the planar structuring process, two basic studies were carried out. On the one hand, the position of the DLIP processing head with respect to the linear stage was kept constant in order to estimate the tolerance of the DLIP process with a different working distance. In comparison, the working distance to the sample surface was kept constant in the second study.

In Figure 34b, the deviation of the structured area per laser pulse in dependence on the angle of inclination γ of the sample is depicted, in terms of length and width of the structured area. The region 1 in Figure 34b represents the acceptable range in which the structured area deviates from the planar reference by a maximum of only 10%. Differently, region 2 represents the area from which significant changes in the structured were observed as the sample surface moves out of the core of the interference volume. Compared to the region 1, the ta-C surface was also structured, but the achievable structure depths are less pronounced. With a constant working distance between the interference build-up and the sample surface, the size of the structured area remains almost constant with increasing angle γ. However, for very large angles of inclination ($\gamma > 12.5°$), an increase in the structural period (from $\Lambda = 2.3$ µm up to $\Lambda = 6.0$ µm) was observed, representing more than 10 % which results from the projection of the interference pattern in the curved surface. The deviation from the spatial period ($\Lambda = 2.3$ µm at $\gamma = 0°$) as a function of the surface tilt angle at constant working distance is shown in Figure 34c.

A further development of the DLIP-setup for structuring the drawing ring radius on industry-related tools was carried out. Due to the lack of rotational symmetry of most of the industry tools, the DLIP laser beams were positioned on the middle of the drawing ring radius (Figure 35b). Therefore the beam path is deflected by a mirror after the last optical element of the DLIP configuration (compare Figure 35a and 35b). During the structuring process, the z-distance of the DLIP optical head is adjusted to the tool geometry and the tool itself is positioned using x-y translational stages. This allows producing the highest structures at the point with the most defavorable tribological conditions (Figure 35c). Surrounding this area, the structures become less pronounced in the entry and exit area of the drawing ring radius (Figure 35d). Furthermore, the computer-controlled adjustment of the mirror angle for a more uniform structure size along the entire drawing ring radius, offers a future research opportunity.

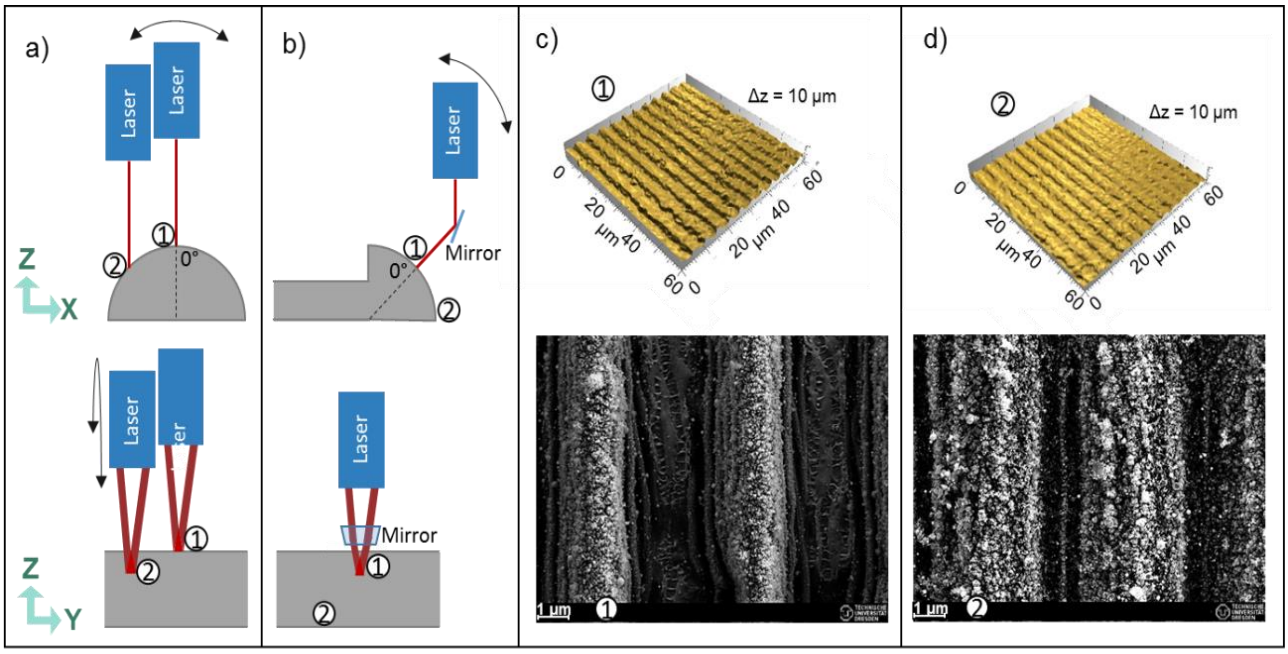

Fig. 35: (a) DLIP setup with vertical laser beam and inclination angle of 0° for structuring of a cylindrical surface and (b) modification of the DLIP setup by placing a mirror between the DLIP head and the pulling edge radius of the dry forming tool. (c, d) Confocal images and SEM images for surfaces corresponding to position 1 and 2 on the half-round surfaces.

4.2 Microstructuring of semi-finished products

While the structuring of the tool surfaces is highly attractive from a tribology and lifetime point of view, the structuring of the semi-finish material is typically not attractive due to its large area. While this is true for nearly all structuring methods, DLIP offers the industrial scalability to achieve structuring speeds of about

0.36 m²/min directly on metal surfaces [58].Such high structuring speeds can be performed by using high power laser systems (e.g. 200W at 1064 nm wavelength). The main objective of the laser treatment is to reduce the effective contact area between the tool and work piece or to control the material flow during a deep drawing application.

Figure 36a summarizes the achievable structure depths of the semi-finished material DC04 as function of the structure periods (Λ = 2.0, 5.0 and 10.0 µm) and the utilized laser fluences. In this case, a high-throughput DLIP setup with a ns-pulsed laser source was used. The results show that the largest structure depths can be achieved for the largest structure periods. However, the highest aspect ratio (AR), defined as the quotient between the structure depth and the spatial period, is achieved for the smaller periods (e.g. AR = 0.3 for Λ = 2.0 µm; AR = 0.1 for Λ = 10.0 µm). Note that the structure depth stagnates for laser fluences higher than ~2 J/cm² in the case of Λ = 2.0 µm. This can be attributed to the excessive melt of the surface, especially for smaller periods due to Marangoni convection [59, 60]. The typical quality of a produced pattern on a DC04 surface is shown in Figure 34b. In this case, the spatial period was Λ = 5.0 µm. The image shows that the line-like periodic structure is well defined all over the steel surface regardless of its initially relatively high surface roughness of about Sz = 10 µm. On the other hand, the processability of non-polished surfaces could be demonstrated, what is necessary for the treatment of real parts.

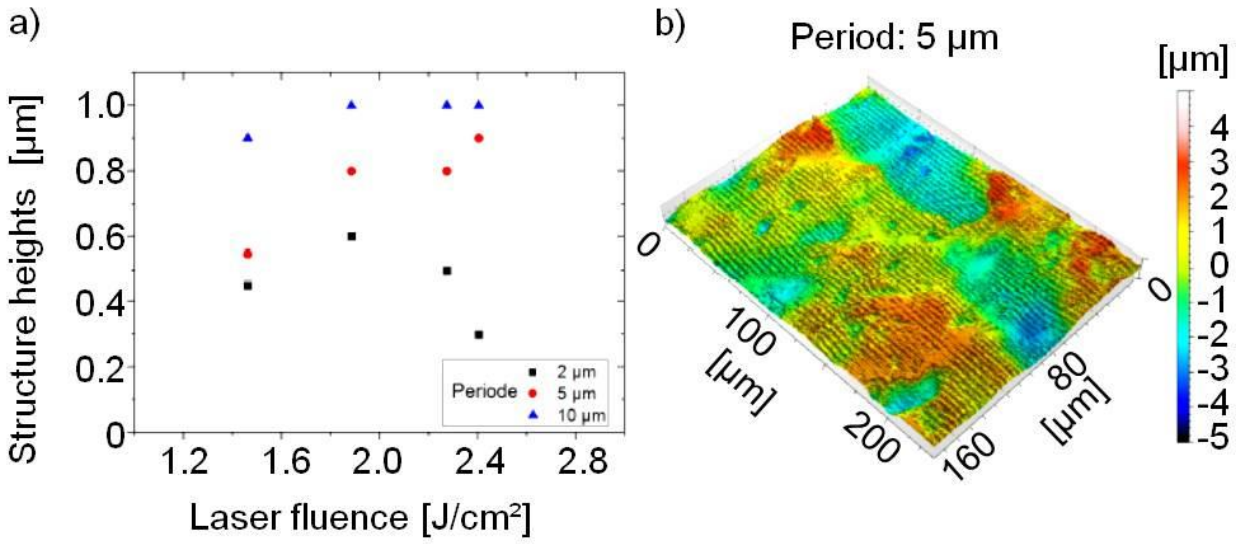

Fig. 36: (a) Structure depth as function of the employed laser fluence for Λ = 2, 5 and 10 µm structure periods (DC04 steel). (b) Surface topology of a DC04 steel surface after DLIP processing with a structure period of Λ = 5 µm (laser fluence: 2.3 J/cm²).

4.2.1 Concept and method optimization for high-speed DLIP of metal sheets

For the fast and effective processing of metal foils, a concept for high-speed structuring was adapted to create functional surface structures on semi-finished sheet metal products. It is based on an optical configuration of two prisms and a cylindrical lens (see Figure 37). Firstly, a biprism is used to generate two partial beams from an expanded and collimated beam of a pulsed high-power laser source. The partial beams are then aligned by a second prism and focused in a line by means of a cylindrical lens (see in Figure 37 the top and side views). In this way, depending on the optical elements used, the resulting line-spot has a lateral dimension between 5 and 15 mm. However, in the direction of processing (x), the length of the spot is only between 50 and 200 µm. Compared to the round laser spot of established DLIP configuration, this allows significantly higher structuring speeds. For instance, throughputs up to 0.36 m²/min on metals have been demonstrated [58]. The spatial period that can be generated is determined by the choice and orientation of the dual prism configuration.

The influence of DLIP microstructuring process of semi-finished products was evaluated using deep drawing tests by strip tensile bending tests. For this purpose, DLIP line structures with a structure period of 10.0 µm were generated on DC04 sheet metal strips and tested in combination with different coating systems (e.g. 3-fold rotationally ta-C coated tools with a coating thickness of 2.25 µm; 1-fold rotationally coated tools with a coating thickness of 4.25 µm).

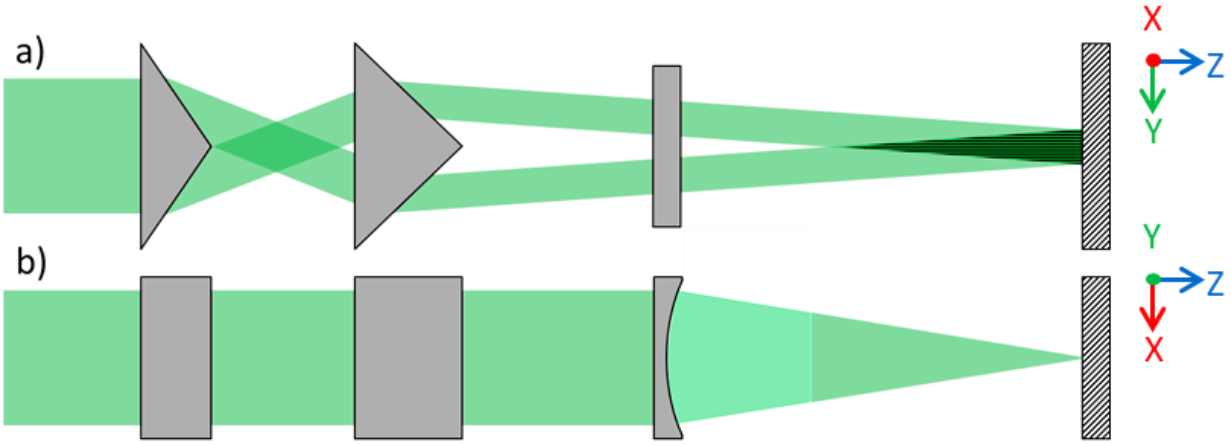

Fig. 37: Optical configuration of the high-speed structuring concept in different side-views: (a) y, z and (b) x, z. The translation of the sample during the structuring process is performed following the x-direction.

In particular in this case, the DC04 sheet metal strips were microstructured with a nanosecond (ns) pulsed laser source with a wavelength of 1064 nm. The extent of the interference area generated on the material with a laser pulse was approximately 0.8 mm² (100 µm x 8 mm). The maximum laser power used was 61 W at a pulse repetition rate of 2 kHz. Figure 36 illustrates the surface condition measured by confocal microscopy before (Figure 38a) and after (Figure 38b) microstructuring. As it can be seen, although the relatively high initial roughness, the produced structures can be very well recognized, which is typical when ns-pulses are used.

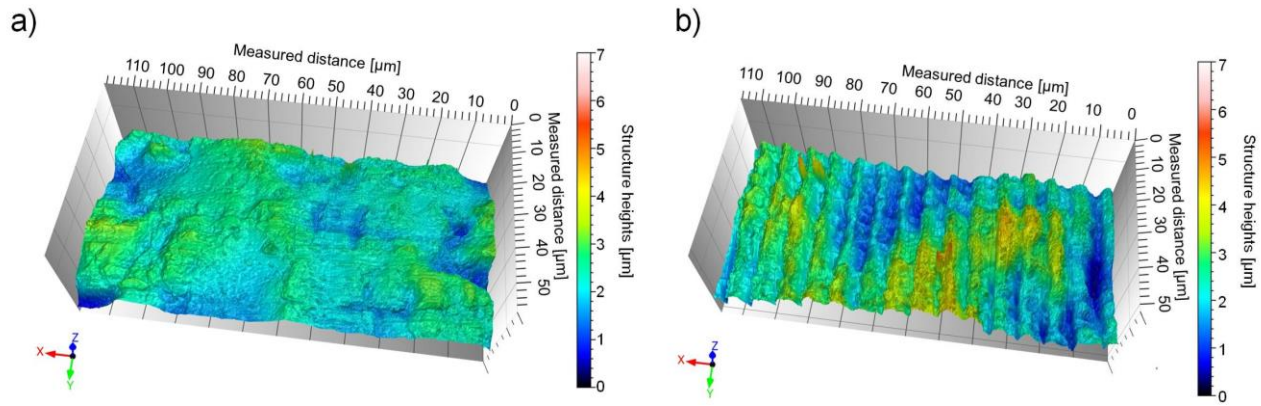

Fig. 38: Surface topography of (a) unstructured and (b) structured DC04 surface. The DC04 sheet metal strips were microstructured with a nanosecond (ns) pulsed laser source at a wavelength of 1064 nm. The maximum laser power used was 61 W at a pulse repetition rate of 2 kHz.

4.2.2 Influence of the DLIP process of DC04 on the friction behavior with a ta-C coated tool

The influence of microstructuring on the friction behaviour in the forming process was investigated by means of draw bending tests. The micro-structuring was performed on commercially-sourced DC04 steel, cut in strips of 1 mm thickness, 1000 mm length and 20 mm width, using the procedure described before. Before structuring, the metal strips were cold-rolled and cleaned using a citrus based cleaner and acetone to remove any prelubrication. One set of 42 strips was left unstructured for reference purpose (Figure 39d). Two types of DLIP structures are produced on the other test strips: one set of 42 strips with structures longitudinal (Figure 39b) and other 42 with structures placed transverse (Figure 39c) to the bending direction.

The structured area on the metal strips was larger than the area in contact with the bending tool in order to ensure a homogenous surface structure influence during the bending procedure. The resulting topography was analysed by confocal microscopy before and after the bend test. The draw bending tests were conducted under dry friction conditions in combination with two different ta-C coated tools (1 and 3-fold rotation during coating procedure). The 9 cylinder-tools with 3-fold rotation coating have a lower ta-C coating thickness of 2.25 µm compared to 9 cylinder-tools with 1-fold rotation coating with 4.25 µm coating thickness. The basic test arrangement of the draw bending test is shown in Figure 39a.

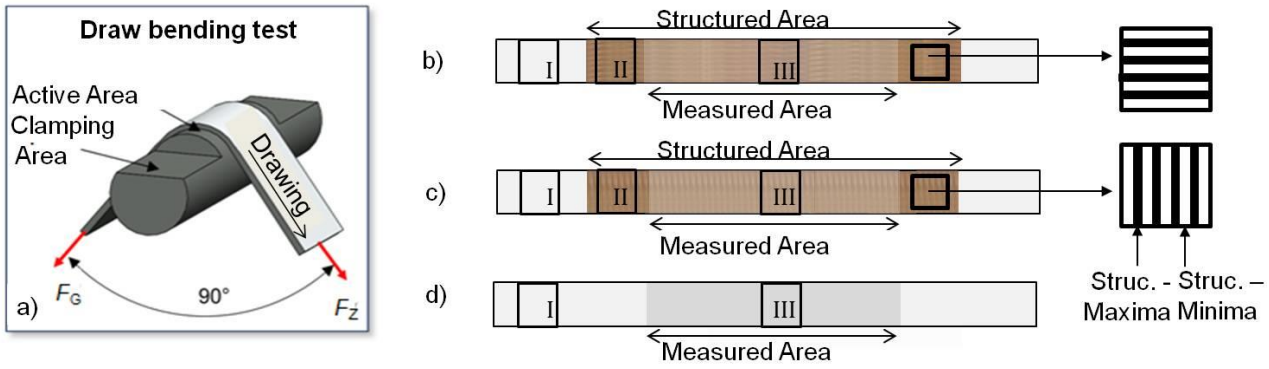

Fig. 39: (a) Draw bending test setup with the metal stripe drawn over the active area of the tool. The metal stripes were differently treated with the DLIP method, obtaining periodic lines which were (b) longitudinal or (c) transversal to the drawing direction. (d) Also the unstructured reference surface was evaluated.

Figure 39b and 29c illustrate the regions corresponding to the measuring positions I, II and III. Area I corresponds to a non-structured region, while Area II was micro-structured but was not in contact with the tool during the bending process. Differently, Area III was micro-structured and was also in contact with the ta-C coated tool during the draw bend test. Figure 39d only shows the areas I (unstructured, outside the tool contact during bending process) and area III (unstructured, with tool contact during bending process).

A statistically secured evaluation of the coefficient of friction was done by 21 measurements for each strip condition (transverse structured, longitudinal structured or unstructured strips) as well as for both tool conditions (1-fold or 3-fold rotation during coating). For each 21 measurement-strips, three cylinders were used which results in 7 stripes for one cylinder. The topographical evaluation of the surfaces after the draw bending test was done with confocal microcopy at several positions in area III.

The evaluation of the coefficient of friction from the bending tests (Figure 40) shows that the laser microstructuring process has an important influence, in particular when the line-like pattern geometry is longitudinal to the drawing direction. This effect was observed, independently of the coating used in the tool (1 or 3 fold coating process). In comparison, all other workpieces, whether with structuring transverse to the drawing direction or without structuring, showed a higher friction coefficient.

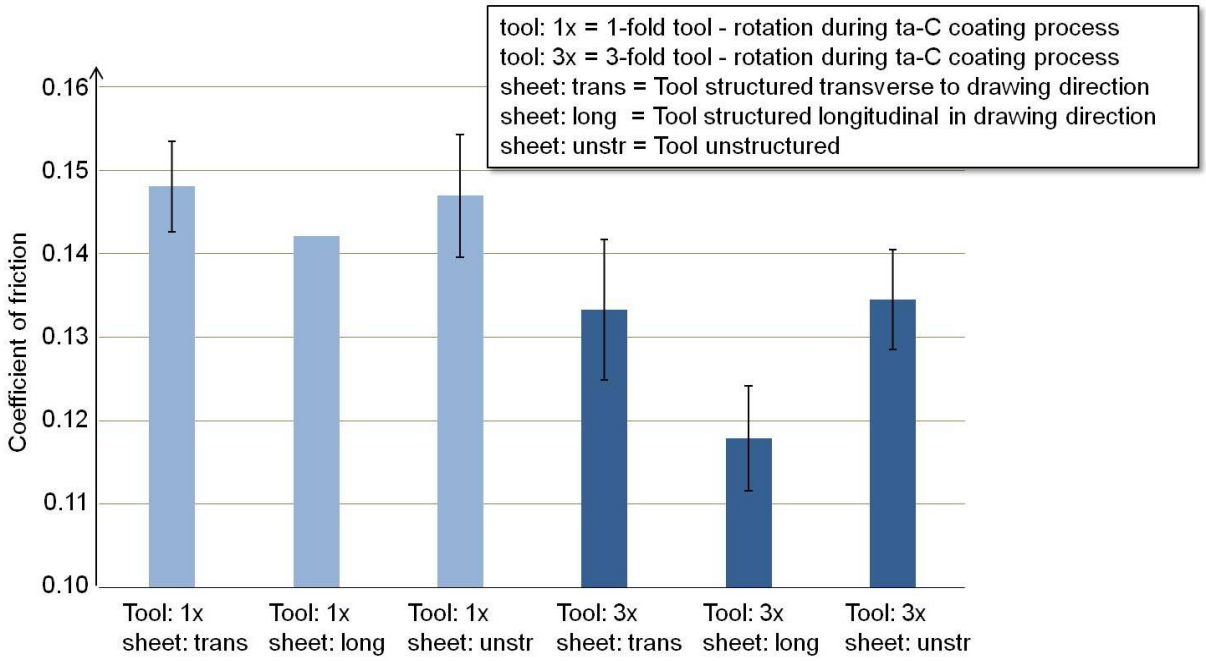

Fig. 40: Coefficient of friction resulting from the draw bend tests for different surface combinations. The lowest friction was measured for the sheet structuring longitudinal in drawing direction and tools with 3-fold rotation during their ta-C coating process.

In addition to the friction coefficient, also the wear behavior of the used strips was evaluated. It was found that the unstructured surface of the reference strips presented significant wear after the bending tests, as former plateaus were abraded (Figure 41c). The DLIP structures on the sheet surfaces transverse (Figure 41a) or longitudinal (Figure 41b) to the drawing direction are still present after the test. In contrast to the unstructured surfaces (Figure 41c), confocal images of the micro structured strips (Figures 41a and 41b) reveal a removal only at the maxima positions of the structured surface pattern on the initial surface plateaus. The DLIP structures at the tribo-contact level, show structure heights similar to those before the test, which means that these structures did not interact during the draw bend test.

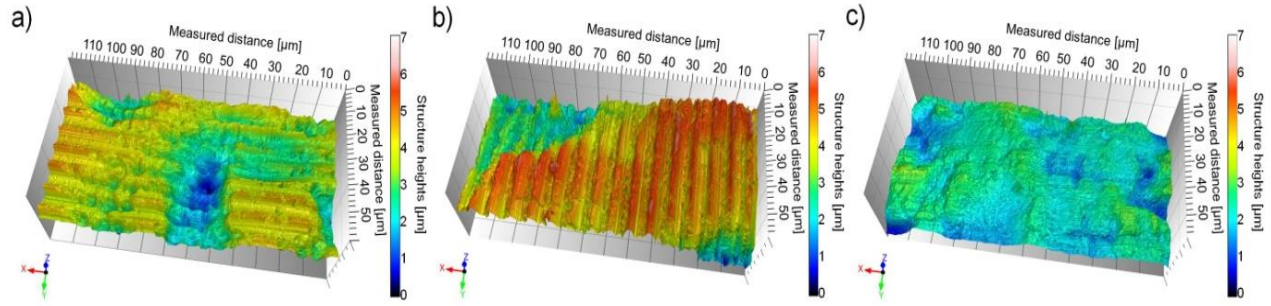

Fig. 41: Surface topographies of the (a) transverse and (b) longitudinal structured surfaces and the (c) unstructured reference surface after the draw bending test.

4.3 Development and optimization of the DLIP-process on industry-close tools

The realization of a load-compatible, lubricant-free deep drawing process requires a significant improvement of the tribological properties, especially at the drawing edge radius. Here the introduction of a microstructure can make a significant contribution. A clear influence of the applied microstructure on the wear behavior of the tools could already be observed in strip tensile bending tests. As a result, a reduction in ta-C coating friction on the tool was observed as a result of the existing microstructure. For this purpose, selected ta-C layer systems (with a hardness of up to ~ 650 GPa) were structured by DLIP.

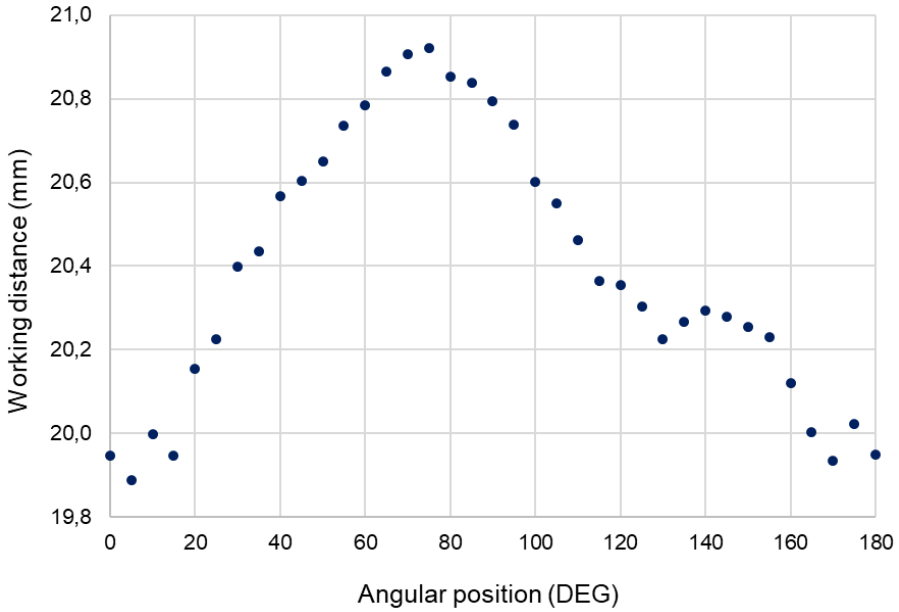

Fig. 42: Relative measured working distance from the DLIP optical head to a cylindrical part as function of the angular position.

A distance measuring system is developed for improved control of the working distance, i.e. the positioning of the DLIP interference volume. This is necessary for the generation of homogeneous microstructures since deviations of several 10 - 100 µm can already lead to minor changes in the projected interference area (2D interference volume on material surface).

The developed system utilized a triangular laser sensor (optoNCDT1320, from Micro-Epsilon Messtechnik GmbH), which was used to register the relative of the DLIP optical module as function of the position. First tests were conducted on cylindrical parts. Thus, the working distance (WD) was measured at different angles of the rotational axis. The measured results are shown in Figure 42, denoting that variations up to 1031 µm, in particular, when the rotational stages are not concentric.

The importance of focus control due to changes in the working distance on a planar surface was analyzed with a tilted steel plate under an inclination angle of 60°. DLIP microstructures were fabricated with a two-beam configuration at 532 nm wavelength, 10 kHz laser frequency and 10 µm distance between the laser pulses. In Figure 43a, images of two structured areas are shown, one with applied distance measuring system during the structuring (left) and one without (right). The microstructures were analyzed every 8 mm along the 40 mm long structured area, at the measuring positions 1 – 5, indicated in the figure. The results for structuring process with distance measuring system can be found in Figure 43 b. In this case, the spatial period was $\Lambda = 4.25$ µm and the structure height was 1.25 ± 0.35 µm for the five positions. In contrast, for the setup without correcting the vertical position of the DLIP head (Figure 43c) the spatial period varied from 1.69 µm up to 7.06 µm and structure height from 0.83 ± 0.58 µm to 1.34 ± 0.43 µm.

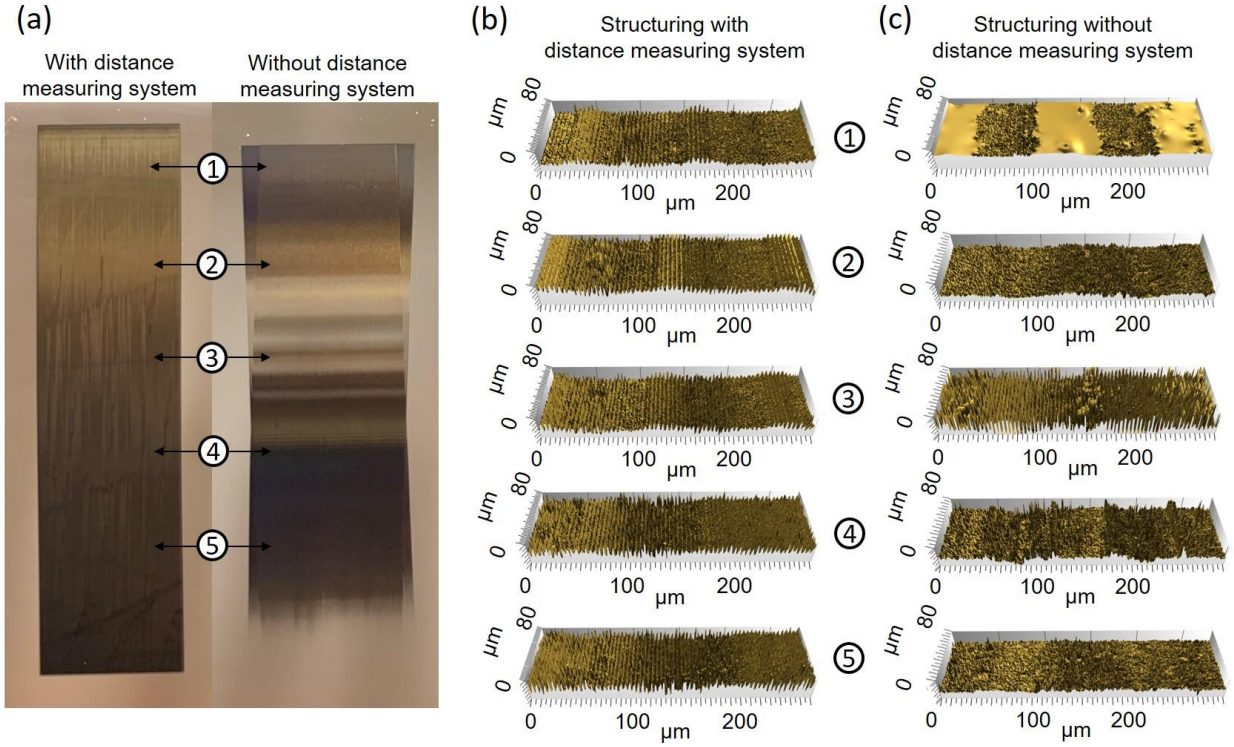

Fig. 43: (a) DLIP structured areas produced on steel surfaces with and without the developed system for working-distance correction using a triangular laser sensor. Confocal images of the treated areas at the positions indicated in (a), (b) using the working-distance adjustment, compared to the standard process (c), without working distance correction.

4.4 DLIP microstructuring of doped ta-C layers to improve tribological properties

The previous microstructures were fabricated on undoped ta-C layers using DLIP processes. Within the scope of a further tribological optimization of the forming tools, doped ta-C layers were also laser treated.

For this tribological test, cylinders were coated with ta-C in different iterations of decoating procedures or the use of nitrogen during the ta-C deposition. The DLIP structuring was done with the setup already shown in Figure 35. This system utilizes a solid-state Nd:YVO4 laser (Edgewave PX 200) emitting 1064 nm wavelength with 10 ps pulse duration and repetition rates up to 30 kHz and maximum output power of 10 W. The spatial period of the microstructuring was $\Lambda = 5.0$ µm.

The tribological tests were performed with a draw bend test machine under 90° deflection. Commercially-sourced D[illegible] metal stripes (like the ones described in the previous section) were drawn over the test cylinders, prepared with the different coated and structured surfaces. The initial surface roughness was Sa = 1.21 ± 0.34 µm The drawn-bend tests were carried out at room temperature under dry conditions with a constant

drawing velocity of 100 mm/s and a contact surface pressure 50 MPa. For each cylinder variation at least two cylinders were evaluated, each with four untreated DC04 stripes bend over them. The drawn length per stripes was 400 mm, resulting in a 1600 mm length drawn over each cylinder.

The results of the friction coefficient measurement can be found in Figure 44. The diagram shows the largest friction coefficient for the untreated, unlubricated reference cylinder surface (0.23). It can be seen, that the friction coefficient of the ta-C + decoated cylinder was 0.16, which means about 30% below the untreated cylinder. A possible explanation is the highly increased value for surface roughness Sa of the coated + decoated surface. The cylinder covered with the ta-C layer exhibited the lowest coefficient of friction (0.135), which is similar to the test results reported in [62]. This value is almost 40 % lower than for the uncoated surface. An iteration of ta-C coating, decoating and repeated ta-C coating leads to an increase of the friction coefficient (0.16), what can be explained by the higher surface roughness of the ta-C surface [61].

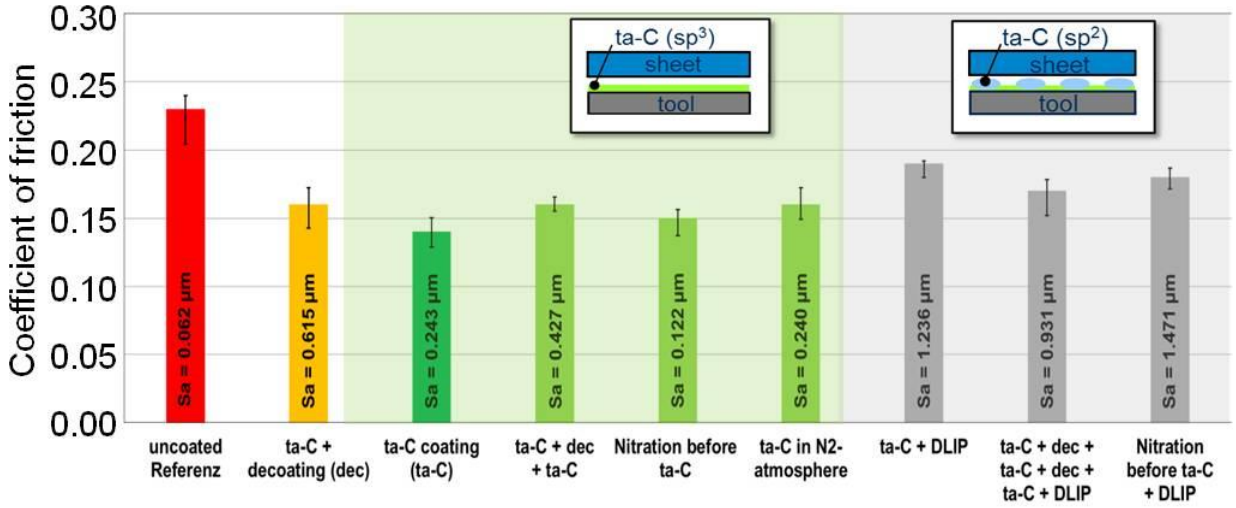

Fig. 44: Measured friction coefficients for differently coated and structured cylinders during draw bend test with DC04 stripes. The surface roughness parameter Sa is shown for better analysis of the dependencies [61].

For the cylinders that were nitride before the ta-C deposition process, the measured friction coefficient was 0.145. This can be attributed to the low surface roughness after nitration and coating. The use of a N_2-atmosphere during the ta-C coating process leads to a friction coefficient of 0.155. The reason for this result can be explained by a lower sp^3-content in the ta-C film. The decrease of the sp^3-content could be attributed to the higher pressures that are used for nitrogen doping (which typically results in an increased sp^2-content).

Friction tests with DLIP structured ta-C coatings show a slight increase in the friction coefficient compared to unstructured ta-C surface. The draw-bend test of the coated and subsequently DLIP-structured tool shows a slightly increased friction coefficient (0.185) which is also similar as previous reported values [62]. This result can be linked to the modified sp^3/sp^2 ration at the interface maxima positions, where sp^2-rich elevations change the contact geometry. The friction coefficient value of the cylinder with repetitive ta-C coating and decoating before the final ta-C structuring was slightly decreased (0.165) compared to the coated and structured sample (0.185). Although the friction coefficients for the laser treated samples increased compared to the ta-C coated samples, a significant reduction in the wear volume is expected [62].

In further experiments, fluorine-doped ta-C coatings (see Chapter 3.3) were microstructured using DLIP. Also in this case, a solid-state Nd:YVO4 laser (Edgewave PX 200) was used, emitting 1064 nm wavelength with 10 ps pulse duration. The spatial period for the microstructuring process was also set to $\Lambda = 5.0$ µm and the pulse overlap to 50 %. In Figure 45 the results corresponding to the structure height analysis as function of the laser fluence on differently doped ta-C surfaces are shown. Furthermore, the insets show surface topographies of selected structured surfaces. The highest structures, with 0.583 ± 0.062 µm were measured on the samples with DLC + 5 sccm CF_4 during the layer deposition. Surfaces with doped DLC + DLC top-layer show structure heights similar to samples with a conventional DLC coating, which can be explained since the doped ta-C layers underneath was not reached by the laser radiation. As the doped DLC samples are only manufactured towards the end of the project, further investigations regarding the influence of the dopant concentration on the triological performance are planned for the future.

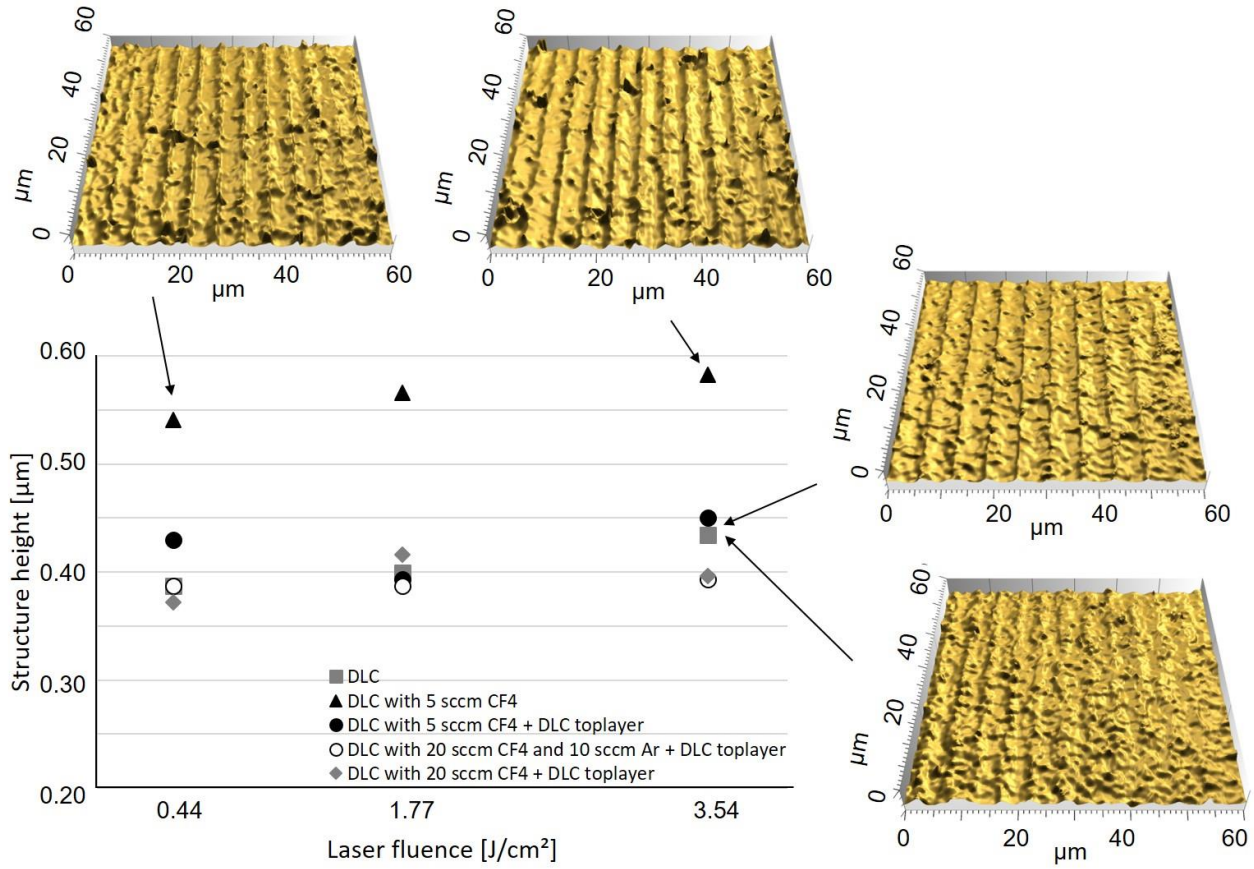

Fig. 45: Measured structure heights of DLIP microstructures on differently doped DLC layers. Small insets depict selected surface topographies.

5 Conclusions

In this project, macroscopic and microscopic structuring approaches were introduced and evaluated to realize lubricant-free deep drawing process, in combination with advanced carbon like diamond coatings (ta-C). The following main conclusions arized from the performed experimental and theoretical calculations and simulations:

Macro-strucring the flange area of deep forming tools reduced the effective friction by minimizing the tool surface in contact with the workpiece to a line or point contact geometry. This macro-structuring concept increased the risk of wrinkling in the unsupported sheet metal areas, since the normally used blank holder force for the stabilization of the process is not available. Thus, the macro-structured blank holder device was slightly immersed in the die. The induced alternating bending in the flange area increased the dent resistance of the semi-finished product in the tangential direction, which neutralized wrinkle formation as well as allowing a significant reduction of the applied blank holder force. For the determination of the punch force, a detailed model to was developed in combination with an analytical buckling analysis for predicting the wrinkle formation. The application of macro-structuring to high strength sheet materials as well as the analysis of the influence of kinematic hardening on the springback behavior of components lead to a lubricant-free deep drawing process under practice-relevant conditions.

Diamond like coatings were also applied to the forming tools in order to reduce friction and wear. This was performed using the spArc-technology. In general, it was observed that the coating deposition process leaded to an increase of the surface roughness. However, it could be also shown that by brushing the ta-C layer, the roughness could be reduced significantly, to values comparable with the roughness of the tools before the deposition process. In order to avoid delamination, graded layers with different hardness levels were satisfactory employed. Alternatively, it was also shown that nitriding of the forming-tools could also significantly increase the adhesion of the ta-C coating. Finally, it was shown that an electrochemical decoating with caustic soda and thus a regeneration of ta-C coated tools is possible. This is of high relevance taking into consideration the high-cost for manufacturing forming tools.

Regarding the microstructuring process of the ta-C coated tools, it was found that the Direct Laser Interference Patterning method produced at low and moderate laser fluences locally rehybridized patterns of sp^2 and sp^3 hybridized carbon areas, having a significant influence in the forming process depending on the processing conditions. The amount of sp^3-sp^2-rehybridization was thereby primarily correlated to the used laser wavelength, laser fluence and laser pulse duration. By applying ultra-short laser pulses (~10 ps), Laser Induced Periodic Surface Structures (LIPSS) were found superimposed on the DLIP-microstructures. For processing industry-close three-dimensional tool surfaces, an optical DLIP setup was constructed. Maximum structure heights of up to 1.4 µm were produced uniformly at the pulling edge radius of the deep forming tool. Also a high-throughput DLIP concept was developed, allowing the optimization and cost-effective microstructuring of metal-sheets to further reduce the friction coefficient down to 0.18 by decreasing the area in contact to the tool surface.

Within this project, a new lubricant-free deep drawing process was developed. Frictional forces and tool wear in critical areas were reduced without the use of standard lubrication by utilizing several strategies, including macro structuring the tool in the flange area, coating of the die edge radius with a protective layer of tetrahedral amorphous carbon (ta-C) and a subsequent micro structuring with DLIP of the ta-C surface and the sheet metals. These outcomes follow the vision of dry metal forming and the targets of the SPP1676 by minimizing the use of lubrication and decreasing the related environmental hazards under practice-relevant conditions.

References

[1] N. Bay, A. Szushima, P. Groche, I. Ishibashi, M. Merklein, M. Morishita, T. Nakamura, S. Schmid, M. Yoshida: Environmentally being tribo-systems for metal forming. CIRP Annals - Manufacturing Technology 59 issue 2 (2010) 760–780.

[2] F. Vollertsen, H. Flosky, T. Seefeld: Dry Metal Forming – a Green Approach, 60 Excellent Innovations in Metal Forming. Springer Vieweg (2015) 113-118.

[3]M. Meier, H. Jaschke: Lubrication of aluminium sheet metal within the automotive industry, Advanced Material Research 6-8 (2005) 551-558.

[4] E. Doege, B.-A. Behrens, B. Springub: Improved analytical model for deep drawing processes of rotationally symmetric cups. Proceedings of NUMIFORM (2004) 844-850.

[5] K. Lange: Handbuch für Industrie und Wissenschaft, Band 2 - Umformtechnik. Springer Verlag Auflage 2 (1990).

[6] F.J. Lenze: Beitrag zum Umformwirkungsgrad beim Tiefziehen. Dissertation, (1982).

[7] E. Doege: Untersuchung über die maximal übertragbare Stempelkraft beim Tiefziehen rotationssymmetrischer zylindrischer Teile. Dissertation (1963) 32–46.

[8] B.W. Senior: Flange Wrinkling in Deep-Drawing Operations. Journal of the Mechanics and Physics of Solids 4 (1956) 235–246.

[9] T.V. Kármán: Untersuchungen über Knickfestigkeit, Mitteilungen über Forschungsarbeiten auf dem Gebiet des Ingenieurswesens. Verein Deutscher Ingenieure 81 (1910) 1-45.

[10] B. Schultrich, P. Siemroth, H.-J. Scheibe: High rate deposition by vacuum arc methods. Surface and Coatings Technology 93 (1997) 64-68.

[11] T. Witke, T.Schuelke, B.Schultrich, P.Siemroth, J.Vetter: Comparison of filtered high-current pulsed arc deposition (φ-HCA) with conventional vacuum arc methods. Surface and Coatings Technology 126 (2000) 81-88.

[12] Y. Pauleau: Residual Stresses in DLC Films and Adhesion to Various Substrates. Tribology of Diamond-Like Carbon Films, Springer (2008) 102-136.

[13] H. Schulz, H.-J. Scheibe, P. Siemroth, B. Schultrich: Pulsed arc deposition of super-hard amorphous carbon films. Applied Physics A 78 (2004) 675–679.

[14] K. Yamamoto, K. Matsukado: Effect of hydrogenated DLC coating hardness on the tribological properties under water lubrication. Tribology International 39 (2006) 1609-1614.

[15] T. Roch, D. Benke, S. Milles, T. Kunze and A. F. Lasagni: Dependence between friction of laser interference patterned carbon and the thin film morphology. Diamond Related Materials 55 (2015) 16-21.

[16] Y. Mabuchi, T. Higuchi, V. Weihnacht: Effect of sp2/sp3 bonding ratio and nitrogen content on friction properties of hydrogen-free DLC coatings. Tribology International 62 (2013) 130-140.

[17] D. Schneider, T. Schwarz, H.-J. Scheibe, M. Panzner: Non-destructive evaluation of diamond and diamond-like carbon films by laser induced surface acoustic waves. Thin Solid Films 195 (1997) 107-116.

[18] D. Liu, G. Benstetter, E. Lodermeier: Influence of the incident angle of energetic carbon ions on the properties of tetrahedral amorphous carbon (ta-C) films. Journal of Vacuum Science & Technology A 21 (2003) 1665-1670.

[19] J. Robertson: Diamond-like amorphous carbon. Materials Science and Engineering: R: Reports 37 (2002) 129-281.

[20] Y. Lifshitz, S. R. Kasi, J. W. Rabalais, W. Eckstein: Subplantation model for film growth from hyperthermal species. Phys. Rev. B 41 (1990) 10468.

[21] E. Rismani, S. K. Sinha, H. Yang, C. S. Bhatia: Effect of pretreatment of Si interlayer by energetic C+ ions on the improved nanotribological properties of magnetic head overcoat. Journal of Applied Physics 111 (2012) 084902.

[22] A. Wasy, G. Balakrishnan, S. H. Lee, J. K. Kim, D. G. Kim, T. G. Kim, J. I. Song: Argon plasma treatment on metal substrates and effects on diamond-like carbon (DLC) coating properties. Crystall research and technology 49, Special Issue: 21st Annual Meeting of the German Crystallographic Society (2014) 55-62.

[23] M. Weber, K. Bewilogua, H. Thomsen, R.Wittorf: Influence of different interlayers and bias voltage on the properties of a-C:H and a-C:H:Me coatings prepared by reactive d.c. magnetron sputtering. Surface and Coatings Technology 201 (2006) 1576-1582.

[24] Z. L. Zhang, T. Bell: Structure and Corrosion Resistance of Plasma Nitrided Stainless Steel. Journal Surface Engineering 1 (1985) 131-136.

[25] C. Li, T. Bell: Corrosion properties of active screen plasma nitrided 316 austenitic stainless steel. Corrosion Science 46 (2004) 1527-1547.

[26] S. Marimuthu, A. M. Kamara, D. Whitehead, P. Mativenga, L. Li: Laser removal of TiN coatings from WC micro-tools and in-process monitoring. Optics & Laser Technology 42 (2010) 1233 – 1239.

[27] T.V. Kononenko, S.M. Pimenov, V.V. Kononenko, E.V. Zavedeev, V.I. Konov, G. Dumitru, V. Romano: Laser-induced spallation in diamond-like carbon films. Applied Physics A 79 (2004) 543–549.

[28] D. Banerjee, A. Jha, K.K. Chattopadhyay: Stable Dispersion of Functionalized Amorphous Carbon Nanotubes in Different Liquids. Journal of Nanofluids 1 (2012) 28-35.

[29] T. Wanheim: Friction at High Normal Pressures. Wear 25 (1973) 225-244.
[30] F.P. Bowden, D. Tabor: Reibung und Schmierung fester Körper, Springer-Verlag (1959)
[31] P. Groche, J. Stahlmann, J. Hartel, M. Köhler: Hydrodynamic Effects of Macroscopic Deterministic Surface Structures in Cold Forging Processes. Tribology International 42 (2009) 1173-1179.
[32] W. Yuanjie: Study of Interface friction reduction using laser micro-textured die surface in metal forming. Ohio state university (2008).
[33] A. Lasagni, M. Seyler, C. Holzapfel, W. Maier, F. Mücklich: Periodical gratings in mixed oxide films by laser interference irradiation. Advanced Materials 17 (2005) 2228-2232.
[34] F. Mücklich, A. Lasagni, C. Daniel: Laser Interference Metallurgy - using interference as a tool for micro/nano structuring. International Journal of Materials Research (Zeitschrift für Metallkunde) 97 (2006) 1337-1344.
[35] A. Lasagni, C. Holzapfel, F. Mücklich: Production of two-dimensional periodical structures by laser interference irradiation on metallic thin films. Applied Surface Science 253 (2006) 1555-1560.
[36] J.M. Carter, R.C. Fleming, T.A. Savas, M.E. Walsh, T.B. O'Reilly, M.L. Schattenburg, H.I. Smith: Interference Lithography. MTL Annual Report (2003).
[37] S. Kuiper, H. van Wolferen, C. van Rijn, W. Nijdam, G. Krijnen, and Elwenspoek: Fabrication ofmicrosieves with sub-micron pore size by laser interference lithography. Journal of Micromechanicsand Microengineering 11 (1) (2001) 33.
[38] J. Bekesi, P. Simon, J. Ihlemann: Determinitsic sub-micron 2D grating structures on steel by UV-fs-laser interference patterning. Appl. Phys. A 114 (2014) 69–73.
[39] T. Roch, E. Beyer, A. Lasagni: Surface modification of thin tetrahedral amorphous carbon films by means of UV direct laser interference patterning. Diam. Relat. Mater. 19 (2010) 1472–1477.
[40] E. Roitero, F. Lasserre, M. Anglada, F. Mücklich, E. Jiménez-Piqué: A parametric study of laser interference surface patterning of dental zirconia: Effects of laser parameters on topography and surface quality. Dent. Mater. 33 (2017) e28–e38.
[41] A.F. Lasagni, T. Roch, D. Langheinrich, M. Bieda, A. Wetzig: Large Area Direct Fabrication of periodic Arrays using Interference Patterning. Physics Proceedia 12 (2011) 214-220.
[42] S. Indrisiunas, B. Voisiat, A. Žukauskas. G. Račiukaitis: Direct laser beam interference patterning technique for fast high aspect ratio surface structuring. In Laser Applications in Microelectronic and Optoelectronic Manufacturing (LAMOM), International Society for Optics and Photonics XX 9350 (2015) 93500.3.
[43] Y. Nakata, M. Yoshida, K. Osawa, N. Miyanaga: Fabricating a regular hexagonal lattice structure by interference pattern of six femtosecond laser beams. *Appl. Surf. Sci.* 417 (2017) 69–72.
[44] A. Lasagni, M. D´Alessandria, R. Giovanelli, F. Mücklich: Advanced design of periodical architectures in bulk metals using Laser Interference Metallurgy. Applied Surface Science 254 (2007) 930–936.
[45] M. Bieda, E. Beyer, A. Lasagni: Direct Fabrication of Hierarchical Microstructures on Metals by meansof Direct Laser Interference Patterning. Journal of Engineering Materials and Technology 132 (2010) 3 031015.
[46] J. Berger, M. Grosse Holthaus, N. Pistillo, K. Rezwan, A. Lasagni: Ultraviolet Laser InterferencePatterning of Hydroxyapatite Surfaces. Applied Surface Science 257 (2011) 3081–3087.
[47] D. Langheinrich, E. Yslas, M. Broglia, V. Rivarola, D. Acevedo, A. Lasagni: Control of cell growth direction by direct fabrication of periodic micro and submicrometer arrays on polymers. Journal of Polymer Science 50 (2012) 415-422.
[48] P.T. Mannion, J. Magee, E. Coyne, G. M. O´Connor, T. J. Glynn: The effect of damage accumulation behaviour on ablation thresholds and damage morphology in ultrafast laser micro-machining of common metals in air. Appl. Surf. Science 233 (2004) 275.
[49] T. Roch, V. Weihnacht, H.-J. Scheibe, A. Roch, A.F. Lasagni: Direct Laser Interference Patterning of tetrahedral carbon films for tribological applications. Diamond Related Materials 33 (2013) 20-26.
[50] H. M. van Driel, J. E. Sipe, J. F. Young: Laser-Induced Periodic Surface Structures on Solids: A Universal Phenomenon. Phys. Rev. Lett. 49 (1982) 1955-1958.
[51] G.R.B.E. Römer, J.Z.P. Skolski, J. Vincenc Oboňa, V. Ocelík, J.T.M. de Hosson, A.J. Huis in 't Veld: Laser-induced periodic surface structures, modeling, experiments, and applications. Proc. SPIE 8968 Laser-based Micro- and Nanoprocessing VIII (2014) 89680D.
[52] J. Yao, C. Zhang, H. Liu, Q. Dai, L. Wu, S. Lan, A.V. Gopal, V.A. Trofimov, T.M. Lysak: High spatial frequency periodic structures induced on metal surface by femtosecond laser pulses. Optics Express 20 (2012) 906.
[53] S. Makowski: Anwendungsnahe Charakterisierung von ta-C Schichten. Diplomarbeit, 2008.
[54] L.G. Cancado, A. Jorio, E.H. Martins Ferreira, F. Stavale, C.A. Achete, R.B. Capaz, M.V.O. Moutinho, A. Lombardo, T.S. Kulmala, A.C. Ferrari: Quantifying Defects in Graphene via Raman Spectroscopy at Different Excitation Energies. Nano Lett. 11 (2011) 3190–3196.
[55] T. Jähnig, A. Lasagni: Laser interference patterned ta-C-coated dry forming tools. Industrial Lubrication and Tribology Vol. ahead-of-print (2020) No. ahead-of-print.
[56] A. Mousavi, M. Schomäcker, A. Brosius: Macro and micro structuring of deep drawing's tools for lubricant free forming. Procedia Engineering 81 (2014) 1890-1895.
[57] M. Bieda, C. Schmädicke, A. Wetzig, A. Lasagni, Direct LaserInterference Patterning of Planar and Non-Planar Steels and Their Microstructural Characterization. Met. Mater. Int. Vol. 19 (2013) 81-86.
[58] A. F. Lasagni, T. Roch, J. Berger, T. Kunze, V. Lang, E. Beyer: To use or not to use (direct laser interference patterning), that is the question. Proc. of SPIE Vol 9351 (2015) 935115-1.
[59] M.C. Tsai, S. Kou: Marangoni convection in weld pools with a free surface. Int. J. Numer. Methods Fluids 9 (1989) 1503.
[60] J.-M. Drezet, S. Pellerin, C. Bezencon, S. Mokadem: Modelling the Marangoni Convection in laser heat treatement. J. Phys. IV France 120 (2004) 299.
[61] T. Jähnig, T. Roch, A. Lasagni: Development in dry metal forming – Structuring ta-C coated tools with Direct Laser Interference Patterning and ultra-short pulsed laser to reduce friction and wear. In Proc. ICALEO (2019).
[62] T. Kunze, A. Mousavi, T. Stucky, F. Böttcher, T. Roch, M. Schomäcker, A. Lasagni, A. Brosius: Tool Optimization for Dry Forming Applications. THe "A" Coatings - 12th International Conference in Manufacturing Engineering (2016) 201-207.